Ti-bearing minerals: from the ocean floor to subduction and back

Inês Pereira, Emilie Bruand, Christian Nicollet, Kenneth T. Koga, Alberto Vitale Brovarone

Ti-bearing minerals: from the ocean floor to subduction and back

Inês Pereira[a*], Emilie Bruand[a,b], Christian Nicollet[a], Kenneth T. Koga[a], Alberto Vitale Brovarone[c,d]

Affiliations

a Université Clermont Auvergne, CNRS, IRD, OPGC, Laboratoire Magmas et Volcans, F-63000 Clermont-Ferrand, France

b Geo-Ocean laboratory, Université Bretagne Occidentale, CNRS, Plouzané, France.

c Dipartimento di Scienze Biologiche, Geologiche e Ambientali (BiGeA), Alma Mater Studiorum Università di Bologna, Piazza di Porta San Donato 1, 40126, Bologna, Italy

d Sorbonne Université, Muséum National d'Histoire Naturelle, UMR CNRS 7590, IRD, Institut de Minéralogie, de Physique des Matériaux et de Cosmochimie, IMPMC, 4 Place Jussieu, 75005, Paris, France

*corresponding author: ines.pereira@dct.uc.pt; present address: University of Coimbra, Department of Earth Sciences and Geosciences Center, Rua Sílvio Lima 3030-790 Coimbra, Portugal

Abstract

Rutile, titanite, and ilmenite are the most common Ti-bearing minerals in metamorphic rocks. Experimental constraints have shown that titanite is stable at low-grade metamorphic conditions, rutile at HP, and ilmenite at HT-LP conditions. Yet, petrological evidence suggests that titanite can also be stable at LT-HP. This implies that both titanite and rutile can be used to develop proxies to track HP metamorphism, which can have interesting applications.

In this study, we have investigated the natural occurrence and chemistry of Ti-bearing minerals in gabbroic rocks that record different degrees of metamorphism, including LP amphibole-bearing gabbros from the ocean floor (Mid-Atlantic and Indian ridge IODP LEGs) and from an obducted ophiolite (Chenaillet) and HP Alpine metagabbros including blueschist and eclogite facies rocks from the Western Alps and Corsica. We have performed detailed petrography and Raman spectroscopy and analysed major and trace elements mineral chemistry using EPMA and LA-ICP-MS.

We found that rutile is stable at low pressure (< 2 kbar) in ocean-floor amphibole-bearing gabbros, lower than experimental constraints had previously suggested. Rutile is also found in eclogitic metagabbros from the Western Alps and can be chemically distinguished from LP rutile. Blueschist metagabbros from the Western Alps and eclogitic metabasalts from Corsica have titanite stable instead of rutile. While the titanite to rutile transition is pressure and temperature dependent, we demonstrate how small variations in bulk-rock Ti/Ca and Ca/Al values within the NCKFMASHTO chemical system may shift their stabilities. High-pressure titanite from these metamafic rocks exhibits La depletion and low La/Sm_N values in comparison to titanite from amphibolite-facies mafic rocks. La/Sm_N or Nb together with Yb and V can be used to distinguish HP titanite from titanite formed under other P-T settings.

These new systematics can be useful in studies using detrital Ti-bearing minerals to probe the HP metamorphic record through time.

Keywords: rutile; titanite; P-T stability; trace element-based discrimination; metagabbro

1. INTRODUCTION

The concept of mineral equilibria has allowed petrologists to estimate pressure and temperature conditions seen by metamorphic rocks (Hoschek, 1969; Burt and Ferry, 1982). However, complete mineral equilibria of rocks are typically unattained during geological processes, especially in coarse-grained rocks that often preserve primary textures, and/or peak and retrograde metamorphic assemblages (non-equilibrium). Over the years, these different snapshots of the rock's evolution have been exploited by petrologists, to better constrain its pressure-temperature (P-T) history. Attribution of a mineral to a pre- or a given metamorphic stage is paramount in reconstructing the P-T evolution of a rock, central to the geodynamic interpretation of metamorphic petrology, and especially for tracing ancient subduction histories (Rubatto, 2002; Engi, 2017; Yakymchuk, 2017).

The "classical" equilibrium thermobarometry approach requires a thorough chemical characterisation of the different mineral phases that attained equilibrium in cation exchange reactions. Alternative ways to this approach have arisen from the development of single grain thermometers (*e.g.* Ti-in quartz, Zr-in-titanite, Zr-in-rutile), allowing to determine temperature conditions from rocks with multiple heritages and/or as inclusions within another mineral. So far, single grain methods are only available for temperature but not pressure, and with known limitations related to uncertainties in elemental behaviour under different P-T conditions and buffering assemblages (Kooijman *et al.*, 2012; Cruz-Uribe *et al.*, 2018; Kendrick and Indares, 2018; Clark *et al.*, 2019). To constrain pressures by single grains, barometry based on quartz Raman spectra have been developed over the last decade, mainly

on quartz in garnet but also on other host-inclusion pairs (*e.g.* Enami *et al.*, 2007; Ashley *et al.*, 2014; Gonzalez, 2019; Cisneros *et al.*, 2020; Gonzalez *et al.*, 2021). Yet, in the absence of quartz inclusions, we need to rely on grain chemistries for an alternative pressure information source.

Titanium-bearing minerals are common accessory minerals in mafic rocks and potentially serve as single grain P-T indicators as referred above. The stability of these minerals, titanite, ilmenite and rutile, are controlled by different factors: system composition, pressure and temperature (Force, 1991; Liou *et al.*, 1998) and fluid composition and its dissolved ions (Spear, 1981; Force, 1991). Rutile is commonly found at higher metamorphic grades, at upper amphibolite and granulite facies (Goldsmith and Force, 1978; Hart *et al.*, 2018), and at high pressures, such as in the eclogite facies or UHP (Liou *et al.*, 1998; Gao *et al.*, 2004; Hart *et al.*, 2016). Rutile is seldom found at lower grades (greenschist facies), and usually associated with fluid alteration processes (Meinhold *et al.*, 2008; Zeh *et al.*, 2018). Titanite, conversely, is mostly found at lower metamorphic grades (greenschist, low amphibolite, blueschist and occasionally eclogite facies conditions; Force, 1991; Vitale Brovarone *et al.*, 2011). Commonly, with increasing metamorphic grade, at upper amphibolite to granulite facies conditions, titanite becomes unstable and ilmenite or rutile replace it (Spear, 1981; Force, 1991; Liou et al., 1998). Ilmenite is favoured by high Fe/Mg bulk-rock compositions (Force, 1991) and medium fO_2 conditions (Spear, 1981; Guo *et al.*, 2017).

Experimental constraints on the stability of these three Ti-phases for MORB compositions are shown in Figure 1a. The lack of experimental data below 600 ºC for mafic compositions has been partly compensated by natural observations and by solution and thermodynamic models of minerals and mineral equilibria (White *et al.*, 2014; Green *et al.*, 2016). Note that the low temperature boundary in Figure 1b is only weakly constrained. Notably, titanite is predicted as more stable than rutile at HP and T <550 °C (Fig. 1b),

although the position of the *titanite-out* reaction changes considerably depending on the choice of solution models (here using the most recent by Green et al., 2016 and White *et al.*, 2014). At lower pressure, titanite and ilmenite are the common Ti-phases (Fig. 1). Yet, the occurrence of rutile-titanite in oceanic gabbros has been reported (Batiza and Vanko, 1985; Mével, 1987; Abe, 2011; Harigane *et al.*, 2011; Rizzo *et al.*, 2019). While titanite presence in these gabbros has been generally linked to the cooling of the oceanic crust during ocean floor metamorphism, the presence of rutile, however, is more puzzling, as it may form due to magmatic or metamorphic processes. Altogether this implies that details on their stabilities at different P-T and chemistry remain puzzling. Until now, despite some attempts to develop trace element-based barometers applied to titanite and rutile (*e.g.* Al-F in titanite – Tropper *et al.*, 2002; Al in rutile – Escudero *et al.*, 2012), no dependency has yet been found (Castelli and Rubatto, 2002; Hoff and Watson, 2018).

In this study we focus on the fate of these Ti-phases from the magmatic stage of the oceanic crust through its subduction. We have investigated the phase stability and trace element systematics of rutile and titanite, two common Ti-bearing metamorphic minerals, which are calibrated as geothermometers, to assess their potential as pressure discriminants. Minor and trace element compositions of accessory minerals have been successfully used in the past to discriminate rock types (e.g. Bruand *et al.*, 2016, 2020; Guo *et al.*, 2020; Scibiorski and Cawood, 2022). By investigating the trace element compositions of these Ti-bearing phases at different metamorphic grades, we explore systematics based on pressure variations. Specifically, we have examined a suite of metamafic rocks with MORB-N affinity (gabbros and basalts) from (i) both the modern and obducted oceanic crust, and (ii) from subducted oceanic crust metamorphosed at blueschist and eclogite facies and exhumed back to upper crustal levels (Fig. 1a and 2). We ultimately investigate which mechanisms control their stability and test if their chemistries change with metamorphic grade. The main purpose is to

provide a novel tool that enables the discrimination of Ti-phases either in or out of petrological context.

2. SAMPLES AND METHODS

2.1. Sampling and Geological settings

Samples come from two different settings: (i) high temperature, low pressure (HT-LP) gabbros metamorphosed during slow seafloor spreading, and (ii) low to medium temperature, high pressure (L/MT-HP) gabbros and basalts metamorphosed during convergent processes. These samples were selected based on their N-MORB-affinity and due to the presence of Ti-phases. HT-LP samples were collected from the Chenaillet Massif, Western Alps (3 samples) and from three different IODP legs, 305 (site U1309D), 209 (site 1271B), both from the Atlantic Ocean Ridge, and 118 (site 735B) in the Indian Ocean Ridge, all with HT amphiboles. L/MT-HP samples were collected from the Western Alps (Queyras, Monviso) and Corsica (San Petrone). More details are given in Figure 2 and Table 1 and the exact sampling locations are given in the Supplementary Data: Electronic Appendix 1.

2.1.1 *International Ocean Drilling Program samples: Atlantic and Indian oceans*

Samples collected from all the following IODP sites and cores are affected by ocean floor metamorphism during gabbro emplacement and cooling of the oceanic crust. Samples used in this study correspond to gabbro that yield a significant oxide content (> 1 %), and metamorphic amphiboles. Preserved metamorphic grades are variable, with some samples preserving a HT metamorphic mineral assemblage with equivalent temperatures of granulite facies whilst others have been re-equilibrated at amphibolite facies conditions. This allows an assessment of the Ti-bearing phase budget present in the oceanic crust before it undergoes subduction and consequent HP metamorphism. More details about the drilling sites and cores can be found in Supplementary Data: Electronic Appendix 1.

144

145 LEG 209, SITE 1271B (0 – 104 m, 15°20'N, 45°00’W)

146 Site 1271 is located along the track of Faranaut 15°N on the western flank of the Mid-Atlantic
147 rift valley. Roughly, 100 m of core were retrieved, corresponding to dunite, harzburgite,
148 troctolite, gabbro, minor gabbronorite, and a small but significant amount of chromitite cm-
149 thick lenses (Shipboard Scientific Party, 2003). Interstitial gabbros in impregnated peridotites,
150 olivine gabbros, and troctolites from Site 1271 include a large proportion of high-temperature
151 amphibole. Samples used in this study, 1316, 1318 and 1320, are all metamorphosed gabbros
152 and were retrieved from cores 3R (piece 19, 18 m depth), 5R (piece 3, 28 m depth), and 8R
153 (piece 5, 41 m depth), respectively, all within Unit I, which was classified as dunite/gabbro
154 (Shipboard Scientific Party, 2003).

155 LEG 305, SITE U1309D (0 – 1645 m, 30°10'N, 42°07’W)

156 Site U1309 is located on the central dome of Atlantis Massif, 14–15 km west of the median
157 valley axis of the Mid-Atlantic Ridge (MAR), where the seafloor coincides with what is
158 interpreted to be a gently sloping, corrugated detachment fault surface (Blackman, 2006). In
159 this site, oxide gabbro (defined by the presence of >2% modal Fe-Ti oxide minerals) makes
160 up about 7% of the rocks recovered. Sample 1319 is an amphibolitised oxide gabbro and
161 corresponds to unit 353, piece 1, recovered at about 662 m depth (Structural Unit II;
162 Blackman, 2006), defined as the Gabbronorite Zone 2 (Blackman, 2006).

163 LEG 118, SITE 735B (0 – 501 m; 32°43'S, 57°16'E)

164 Site 735 is located on a shallow platform, on the east rim of the Atlantis II Transform located
165 in the magnetic anomaly equivalent to about 12 Ma (Robinson *et al.*, 1991). This platform,
166 about 9 km long in a north-south direction and 4 km wide, is one of a series of uplifted
167 blocks. A total of 435 m of olivine gabbro, olivine-bearing gabbro, two pyroxene gabbro,

iron-titanium oxide gabbro, troctolite, and microgabbro with rare basalt and trondjhemite was recovered from Hole 735B. These rocks have undergone varying degrees of plastic and brittle deformation, and many have well-developed foliations. The sample used in this study (5450) is a metamorphosed oxide gabbro and comes from unit VI, core 85R, section 4, corresponding to piece 1E of the original log and to approximately 475m depth. The unit this sample comes from corresponds to olivine-rich gabbro having frequent layers of troctolite (Robinson et al., 1991). Frequent intervals of gabbro are characterized by mylonitic to porphyroclastic textures, the latter corresponding to the collected sample.

2.1.2. *The Liguro-Piemontese domain in the Western Alps and Corsica*

The Piemonte-Liguria domain in the Western Alps represents the westernmost part of the Alpine arc and extends to Corsica in the south (Fig. 2 A, B). This domain is interpreted as a remnant of the accretionary wedge, where oceanic sediments and relics of oceanic lithosphere are accumulated (Marthaler and Stampfli, 1989; Deville *et al.*, 1992; Agard *et al.*, 2001). In the Piemonte-Liguria zone we studied two areas: (i) a west-east transect going from the obducted ophiolite in the Chenaillet Massif, to the blueschist Queyras/Combin unit towards the eclogitic Viso/Zermatt unit, and (ii) Alpine Corsica in the San Petrone Mount area. Together, these samples allow a comparison between what constituted the pre-Alpine oceanic lithosphere crust (preserved in the Chenaillet ophiolite as the least metamorphosed past of the Western Alps) and oceanic lithosphere units that underwent subduction and metamorphism at different depths during the Alpine orogeny.

Chenaillet Massif. The Chenaillet amphibole-bearing gabbros were long interpreted as corresponding to obducted amphibole-bearing gabbros recording ocean floor metamorphism (Mevel et al., 1978). They formed in the Piemonte-Liguria basin during the Jurassic, and were so far described as negligibly affected by Alpine metamorphism (Manatschal *et al.*, 2011 and

192 references therein). Recent work by Corno *et al.* (2023) describe for the first time the presence
193 HT assemblage along with remnant of Alpine HP assemblages (e.g. lawsonite, omphacite) in
194 some of the gabbros and volcanics, questioning the interpretation of previous authors
195 implying the obduction of the Chenaillet massif. HP alpine metamorphism (presence of
196 lawsonite and omphacite) were not observed in the studied gabbros. Recent ages obtained
197 from magmatic zircon in the studied gabbros yield crystallisation ages of around 161 ± 0.8
198 Ma (Nicollet et al., 2022). In this locality, three amphibole-bearing gabbros have been
199 sampled (Table 1).

200 *Queyras and Monviso Massifs*. The blueschist-facies Queyras and eclogite-facies
201 Monviso metaophiolite units consist mainly of meter to kilometer-sized metagabbroic lenses
202 included in metasediments (Schistes Lustrés complex; SL) and/or serpentinite with
203 ophicalcite (Ballèvre *et al.*, 1990). Magmatic ages of the Monviso eclogite protoliths have
204 been determined using coupled zircon U-Pb and trace element chemistry to 163 ± 2 Ma
205 (Rubatto and Hermann, 2003). In the Western Alps, the subduction stage started during the
206 late Cretaceous at around 80 Ma (e.g. Rubatto *et al.*, 2011) and lasted until at least 45 Ma
207 (Rubatto and Hermann, 2003). A west-east transect across the Queyras and Monviso units is
208 affected by a HP-LT metamorphic event, which increases towards the East from blueschist (8-
209 14 kbar; 350-450°C) to eclogite facies conditions (up to 20 kbar; 450-500°C) (Blake and
210 Moore, 1995; Agard et al., 2001; Schwartz, 2002; Schwartz *et al.*, 2013). The Liguro-
211 Piemontese units are partially retrogressed into greenschist facies conditions along an
212 isothermal retrograde path (Caby, 1995), but fast exhumation, probably combined with
213 restricted fluid circulation, favoured the preservation of the peak metamorphism assemblages
214 (Rubatto and Hermann, 2001; Angiboust and Glodny, 2020).

215 Across the Queyras and Monviso, different localities where HP metagabbros occur
216 have been sampled: (i) three lawsonite blueschist from Sommet Bucher (Q1), Vallon de

Clausis (Q6) and Tour Réal (TR10); ii) three eclogite from Verne (VE29), Passo Gallarino (PG) and Lago Superiore (LS). Sampling details can be found in Table 1 and full petrographic descriptions in section 4.

Alpine Corsica. The schistes lustrés (SL) units in Corsica have undergone lawsonite blueschist- to lawsonite eclogite-facies metamorphism during the Alpine orogeny and suffered variable retrogression to the greenschist facies (Fournier *et al.*, 1991; Vitale Brovarone *et al.*, 2011; Vitale Brovarone and Agard, 2013; Vitale Brovarone and Herwartz, 2013). Mafic eclogites found in the SL have N-MORB affinity (Saccani *et al.*, 2008). Ages of gabbros from the oceanic units have been constrained using Sm-Nd isochrons to 162 ± 10 and 159 ± 15 Ma (Rampone *et al.*, 2009). HP metamorphism affecting these units has been dated using a Sm-Nd isochron yielding 84 ± 5 Ma (Lahondère and Guerrot, 1997), but more recent studies have clearly demonstrated that HP metamorphism in the SL took place during the Late Eocene (37 – 34 Ma) (Vitale Brovarone and Herwartz, 2013).

Two samples were selected for this study that were collected from similar areas to the ones figuring in Vitale Brovarone et al. (2011) (samples OF3158 and OF3310) from the San Petrone Mount in Corsica. These correspond to coexisting lawsonite eclogite and blueschist eclogite rocks equilibrated at the same P-T conditions of 520 ± 20 ºC and 23 ± 1 kbar (Vitale Brovarone et al., 2011).

2.2 Methodology

2.2.1 Whole-rock geochemistry

Eclogite VE29 and some selected blueschist samples (Supplementary Data: Electronic Appendix 1) were crushed using a jaw crusher and pulverised using the sample preparation facilities at the Laboratoire Magmas et Volcans (LMV), Clermont-Ferrand (France) to obtain major element compositions. Bulk rock major elements of these samples were analysed using

241 a Jobin-Yvon ULTIMA Inductively Coupled Plasma-Atomic Emission Spectroscopy at the
242 LMV, following similar analytical and instrumental procedures to the ones reported in Barette
243 et al. (2017) and Guitreau et al. (2019). Bulk-rock major and minor element compositions of
244 IODP samples were compiled from the IODP data repository. Bulk rock available on Corsica
245 eclogites were compiled from Vitale-Brovarone et al. (2011). All whole-rock data can be
246 found in the Supplementary Data: Electronic Appendix 1.

247 *2.2.2 Scanning Electron Microscopy*

248 Most collected samples were fist-sized and therefore only minerals from polished thin section
249 were analysed during this study. Ti-bearing minerals were identified and imaged to reveal
250 internal zoning or inclusions using Scanning Electron Microscopy (SEM) sessions at the
251 LMV using a JEOL JSM-5910 LV with a tungsten filament and 15 kV accelerating voltages
252 for backscatter electron imaging (BSE).

253 *2.2.3. Raman Spectroscopy*

254 To determine TiO_2 polymorphism we used a Renishaw InVia confocal Raman micro-
255 spectrometer equipped with a 532 nm diode laser (200 mW output power) and a CCD
256 detector and a Leica DM 2500 M optical microscope at the LMV. A 100× objective in high
257 confocality setting (slit aperture of 20 µm) was used and the range of power applied was
258 always lower than 1% of the laser energy. Acquisition time was set at 10 s, and 5
259 accumulations.

260 *2.2.4. Electron Probe Microanalyses*

261 Silicate and Ti-mineral phase minerals were analysed for major, minor and occasionally trace
262 elements with a CAMECA SX100 electron probe microanalyser (EPMA) at LMV. Variable
263 analytical conditions were used to target different elements for the different minerals of
264 interest. A detailed instrumental and analytical setup for each session can be found in the

Supplementary Data: Electronic Appendix 1. For silicate mineral characterisation the following elements were determined: Si, Ti, Al, Mg, Fe, Mn, Ca, Na, K, and Cr. Data can be found in Supplementary Data: Electronic Appendix 2. For Ti-mineral phases, the following elements were part of different analytical sessions: Si, Ca, Al, P, Ti, Mn, Fe, Cr, F, Zr, Nb, La, Ta, Y, Sc, Sn, V. Khan titanite reference material (Heaman, 2009) was used for quality control monitoring during Ti-mineral phase analyses. Supplementary Data: Electronic Appendix 3.

2.2.5. Laser Ablation-Inductively Coupled Plasma Mass Spectrometry

Further trace elements chemistry of titanite, rutile and ilmenite was obtained using laser ablation-inductively coupled plasma mass spectrometry (LA-(HR)ICPMS) using the Resonetics Resolution M-50E 193 nm excimer laser coupled to the Thermo Element XR at LMV daily calibrated and optimised using NIST612.

The spot sizes used ranged between 9 and 27 µm with a repetition rate of 1 to 2 Hz and a fluence of 2.5 to 3 J/cm^2. Each analysis consisted of 20s background and between 50 and 90s of signal acquisition. More details can be found in the appendix. We used a sample bracketing method using GSE-1G and GSD-1G as primary standards and GSC-1G, GSD-1G or BHVO in the middle of the sequence as secondary standards (Jochum et al., 2005). Khan (Heaman, 2009) was also used as a secondary reference material for additional quality control. Details on the isotopes that were measured, data processing and quality control can be found in Supplementary Data: Electronic Appendix 1, 3 and 4.

3. RESULTS

3.1. Petrography

3.1.1. Modern oceanic crust amphibole-bearing gabbros

Amphibole-bearing gabbros. All samples (1316, 1318, 1320, 1319 and 5450) correspond to coarse-grained gabbro, with primary clinopyroxene and plagioclase. Overall, plagioclase is the most abundant mineral phase (40-65%) but is either strongly or slightly altered to secondary plagioclase (albite), quartz and variable chlorite/sericite (Fig.3-A). Relict magmatic clinopyroxene (augite in composition) has reacted with plagioclase to produce brown hornblende-edenite coronas around it (1320, 5450, 1316) together with albite and epidote. In samples 1319, 5450 and 1316, brown amphiboles are then replaced or overgrown by green hornblende and in 1319 also by actinolite + chlorite. Accessory minerals (< 3 %vol) correspond to ilmenite, titanite, rutile and occasionally hematite, mostly associated to amphibole. In all samples, preserved disequilibrium mineral assemblages are found. Due to the variable presence and proportion of brown and green amphiboles in these samples, there is a spectrum from sample 1320, which records granulite facies conditions with a brown amphibole found as idioblastic crystals and in equilibrium with plagioclase, to samples 5450, 1318 and 1316 that have suffered partial retrogression to the amphibolite facies, and sample 1319 that has completely retrogressed to lower amphibolite/upper greenschist facies conditions. Despite not constituting the most robust estimate, Ti-in-amphibole thermometry (Otten, 1994) applied to two endmembers of these units, samples 1320 and 1319, yield temperatures compatible with metamorphism under the granulite facies (840 to 740 °C) and amphibolite facies (590 °C), respectively (Supplementary Data: Electronic Appendix 2), providing a working frame for metamorphic conditions at which we find the Ti-phases.

Ti-bearing mineral assemblage. Titanite is the most ubiquitous Ti-bearing mineral in all the metagabbro samples. It commonly forms coronas around an earlier Ti-bearing mineral phase (Fig.3-A-F), often ilmenite (Fig.3-C), more rarely rutile (Fig.3-A, B) or around both (Fig.3 D to F), but it can also occur as idioblastic crystals under amphibolite conditions (Fig.3-G,H). In sample 1320, rutile occurs as grains typically between 50 to 100 µm in size,

313 associated with brown hornblende and within ilmenite-rutile-titanite aggregates (Fig.3-D). In
314 samples recording a lower temperature retrogression (sample 1316 and 1319), ilmenite is
315 surrounded by coronas formed by titanite and rutile showing some host crystallography-
316 controlled growth (Fig.3-D). In this case, titanite and rutile replace ilmenite during cooling to
317 amphibolite or greenschist facies conditions, illustrating its disequilibrium (Fig.3-E-F). In
318 summary, whilst in cases titanite and rutile form intergrowths in coronas around ilmenite,
319 with rutile showing some host crystallography-controlled growth (Fig.3-D), there are also
320 cases where rutile is found as coarser (20 to 50 μm), sub-spherical inclusions within ilmenite
321 (Fig.3-D-F) or, more rarely, as single grains, up to 100 μm large, directly overgrown by
322 titanite (Fig.3-A,B). While the core of some of these complex grains, formed by either
323 ilmenite or rutile, corresponds to at least granulite conditions, the titanite replacement (+ rutile
324 lamellae) or new crystals growth takes place at lower grade conditions, during cooling to
325 amphibolite or greenschist facies conditions. Ilmenite in these metagabbro rocks can either be
326 of magmatic origin or recrystallised during ocean floor metamorphism. In this way, we have
327 three (but continuous) metamorphic stages: i) augite, plagioclase and brown hornblende +
328 ilmenite/rutile, followed by ii) green hornblende, plagioclase +/- rutile, and a iii) actinolite,
329 albite, chlorite + titanite (+/- rutile lamellae).

330 *3.1.2. Western Alps obducted metagabbros*

331 These samples were collected from highly heterogeneous outcrops in the Chenaillet Massif,
332 where a coarse-grained texture is preserved, but occasionally amphiboles reach several
333 centimetres, and deformation variably affects these units, from highly sheared to non-
334 deformed.

335 *Amphibole-bearing gabbros.* Three samples from the Chenaillet were examined, two
336 corresponding to a gabbro composition (Ch1 and Ch3) and one interpreted as more dioritic

(ChDi). ChDi primary mineral assemblage has been replaced by a pale green amphibole, albite, sericite, epidote and chlorite, and primary ilmenite is overgrown by titanite ± rutile. Fe-Ti oxides make up more than 3 wt% and have no preferred textural association to any major rock forming mineral. The two samples of gabbroic composition are very similar, and the predominant mineral assemblage corresponds to albite (secondary) and amphibole (Fig.4-A), but while Ch1 has preserved relict of clinopyroxene (augite), in Ch3 all clinopyroxene have been replaced by amphibole. There are three different Ca-amphiboles: brown edenite or hornblende, brown-green hornblende and green actinolite (Fig. 4). All amphiboles have less than 0.5 Ti apfu, and they range in Al^{iv} = 0.35 – 1.51, and Na_{M4} = 0.04 – 0.52 (Supplementary Data: Electronic Appendix 2). Brown amphibole is either arranged as overgrowths on destabilised magmatic clinopyroxene (Fig.4-A) or as large (> 0.5 mm) xenoblastic crystals (Fig.4-B). These represent the main high-temperature mineral assemblage successively replaced during subsequent recrystallisation along their edges by a brown-green and then a green amphibole arranged as a corona texture. The break down of the Ti-bearing amphiboles caused the release of Ti and the growth of the titanite and rutile. Maximum TiO_2 concentrations in Ch1 amphiboles reach 2.62 to 3 wt% while in Ch3 they reach 3.02 to 3.07 wt% (Supplementary Data: Electronic Appendix 2), yielding temperatures between 890 and 790 °C (Ch1) and 940-930 °C (Ch3; Supplementary Data: Electronic Appendix 1) (Otten, 1984). These conditions comfortably indicate temperatures typical of granulite facies metamorphism even if the amphibole thermometer may have poor accuracy. A corona of brown-green amphibole develops around these brown amphiboles, which are either hornblende (725 to 600 °C; 0.3 – 1.73 wt% TiO_2) or actinolite (610-570 °C; 0.5 wt% TiO_2), and to which titanite grains are associated with (Fig.4-A-C). Similarly to oceanic gabbros, a partial preservation of primary magmatic minerals towards granulite and amphibolite facies conditions was likely acquired during cooling of these units at the oceanic ridge.

362 *Ti-bearing mineral assemblage.* Titanite is the stable metamorphic Ti-phase in all the
363 amphibole-bearing gabbros, and ilmenite in the metadiorite. Titanite can be found in two
364 types of associations: (i) commonly as small grains (< 20 µm) at the transition between brown
365 and green hornblende (Fig.4-B-C); or (ii) more rarely as hypidioblastic grains (up to 80 µm in
366 size) associated with actinolite in later veins (Fig.4-G, H). Although the former is
367 homogeneous in BSE, the latter shows strong BSE zonation (Fig.4-H). Ilmenite is more
368 common in the ChDi than in the other metagabbros, where grains are often replaced by rutile-
369 titanite association (Fig.4-D-F). In this case, rutile either occurs as coarse grains of up to 25
370 µm or as very fine grains, often showing preferred crystallographic orientation. Both coarse
371 and lamellae rutile are common, easily found in multiple sites in this sample. Rutile lamellae
372 develop at 60º/120º angles with ilmenite (Fig.4-E,F), and they seem to indicate topotactic
373 replacement of ilmenite, such as described by Force et al. (1996), during titanite growth, with
374 excess Ti forming rutile. No evident BSE zonation was identified.

375

376 3.1.3. *Alpine blueschist and eclogite*

377 Nine samples were collected from the Western Alps and Alpine Corsica localities. These units
378 are usually enclosed in HP metapelites and marls.

379 *Blueschist (LT, HP)*

380 Metagabbros - QE-1, QE-6, TR10. These blueschist rocks all located in the Queyras
381 valley preserve their original gabbroic texture, where both pyroxene and plagioclase sites can
382 be recognised despite the development of Alpine foliation. The HP mineral assemblage is
383 given by glaucophane, lawsonite, albite and titanite ± epidote and secondary minerals present
384 are actinolite ± chlorite. Primary magmatic clinopyroxene has been nearly all replaced by
385 glaucophane, although it is still recognisable (Fig. 5-A). The original magmatic plagioclase

site is replaced by lawsonite and some epidote and albite aggregates (Fig. 5-A,B). TR10 sample is richer in blue-amphibole, with compositions ranging from ferroglaucophane to riebeckite (Supplementary Data: Electronic Appendix 1 and 2), whereas blue amphibole in QE-1 and QE-6 is glaucophane. These amphiboles are variably replaced by actinolite (Fig.5-B).

Ti-bearing mineral assemblage. In these metagabbros, the stable Ti-bearing mineral is titanite. Titanite is found as large and elongated stripes of xenoblastic crystals (100's μm) between the clinopyroxene and plagioclase sites, and it also occurs as coronas, probably formed at the expense of leached Ca and Ti from former pyroxene and Ca-rich plagioclase (Fig. 5-A). Titanite also occurs together with glaucophane and lawsonite ± albite. Occasionally, it is possible to identify tiny rutile inclusions (< 10 μm wide) in the core of larger (> 400 μm) titanite grains (Fig. 5-C-F), arranged as spotted texture within titanite. In places where only smaller titanite grains are found, fully recrystallised at blueschist conditions, rutile was absent. No evidence of rutile being in equilibrium with other blueschist facies minerals was observed. Ilmenite is also absent and no visible BSE zoning in titanite was identified.

Eclogite-facies rocks (M/LT, HP)

Metagabbros - VE-29, LS and PG samples. PG is a metagabbro that still preserves its primary mineralogy, with about 50:50 proportion of clinopyroxene and plagioclase sites. A primary clinopyroxene (augite) is found, with very light brown to greenish colour. The plagioclase site is replaced by quartz, chlorite, zoisite and phengite. Rutile and titanite are accessories and form elongated bands (Fig. 6-A). Amphibole occurs as very small (<20 μm) idioblastic grains associated to zoisite and epidote. This seems to occur as thin veins/films infiltrating the metagabbro. Garnet is not observed. This sample have mostly preserved its magmatic texture

and although no omphacite was clearly observed, this rock was sampled from the classical locality in Passo Gallarino where other eclogites have been previously sampled. The exact location is given in the Supplementary Data: Electronic Appendix 1.

VE-29 was collected in Verne locality and is a metagabbro with a granoporphyroblastic texture composed of omphacite, phengite, garnet, quartz, and rutile ± ilmenite ± epidote from the Viso unit (Groppo and Castelli, 2010; Fig. 6-B). Garnet porphyroblasts (up to 500 μm) are almandine-rich and exhibit an increase of Fe and Mg contents towards the rim, similarly to Groppo and Castelli (2010). Garnet includes a significant number of rutile inclusions, many of which are overgrown by a thin rim (<2 μm) of ilmenite. Paragonite and epidote are also frequently found as mineral inclusions. Omphacite is occasionally associated with phengite. These can be altered to chlorite, and some chlorite is also found in garnet fractures.

LS was collected in Lago Superiore area and corresponds to a strongly foliated eclogite with granoblastic texture, composed by omphacite, garnet and rutile (Fig. 6-C). Garnet grains are hypidioblastic but of small size (< 500 μm) and frequently strongly zoned, with Ca-richer almandine cores and Mg-richer almandine rims (cores: $Alm_{55}Grs_{33}Sps_{07}Prp_{05}$; rims: $Alm_{67}Prp_{19}Grs_{13}Sps_{01}$; Angiboust et al., 2012). In similar eclogite retrieved from Lago Superiore (Angiboust et al., 2012), three omphacite generations, with variable compositions, could be identified.

Ti-bearing mineral assemblage. In all metagabbroic rocks (PG, VE29, LS), rutile is the stable Ti-phase. Rutile grains can be large (200-300 μm), sub-spherical and with brown-amber colour in plane polarised light. In PG, rutile can be found as coarse, sub-spherical grains in aggregates or individual crystals dispersed in the matrix. Some of these are overgrown by titanite (Fig. 6-A) that was probably formed during decompression from

eclogitic conditions (Schwartz et al., 2000). Rutile from VE-29 ranges in size from 20 to 200 μm, hypidioblastic individual grains that can be found included in garnet or dispersed in the matrix between omphacite grains. Rutile always displays Fe-exsolution along its cleavage. Less frequently, ilmenite overgrowths are seen. Larger rutile grains which are mostly hosted in the garnet porphyroblasts (Fig. 6-B) often preserve mineral inclusions, such as omphacite, epidote and more rarely apatite. Rutile grains in LS are of variable size (> 300 to < 100 μm) and frequently occur as bands of rutile aggregates (Fig. 6-C), aligned along the main foliation, together with garnet and omphacite. These occur as aggregates of 50-200 μm, idio- to hypidioblastic grains, forming stripes/bands. These rutile grains have a brown-honey colour. They also occur as inclusions within garnet, but more frequently found along grain boundaries. Ilmenite exsolution bands or overgrowth around rutile are frequent, although these tend to be thin (< 2 μm width; Fig. 6-D). Rutile grains from these metagabbros show no BSE zoning.

Metabasalts - C16 sample. This sample is equivalent to sample OF3310 in Vitale Brovarone et al. (2011). It corresponds to a foliated lawsonite-bearing "blueschist" eclogite (Fig. 6-E) with an associated omphacite- and garnet-bearing vein (C16v; Fig. 6-F). The sample paragenesis is glaucophane, lawsonite, quartz, albite, titanite, and Fe-Ti oxides (Fig. 6-E). The vein, which is ca. 1 cm wide; contains omphacite, garnet, lawsonite, glaucophane, albite and titanite (Fig. 6-F). Both parts reached the same P-T conditions, but paragenesis is dependent on the bulk composition of the basalt and the vein (Vitale Brovarone et al., 2011). P-T conditions are constrained by the lawsonite-blueschist eclogite from Vitale Brovarone et al. (2011) yielding 520 ± 20 ℃ and 23 ± 1 kbar. *C147 sample*. This sample is equivalent to OF3158 in Vitale Brovarone et al. (2011) and corresponds to a lawsonite-bearing eclogite (Fig. 6-G), with occasionally preserved magmatic textures. The HP paragenesis is garnet, omphacite, lawsonite, glaucophane, titanite and late Fe-Ti oxides. Garnet can be idio- to

459 hypidioblastic, usually small in grain size (<500 μm). P-T conditions are similar to those of
460 C16 (Table 1).

461 *Ti-bearing mineral assemblage.* In C16, only titanite is found as the main Ti-host
462 phase. Titanite grains are abundant, hypidioblastic, but small (<20 μm), and become more
463 frequent and larger in the vein that crosscuts the basalt (Fig. 6-F). In C147, titanite is the only
464 Ti-mineral phase, occurring as small grain size idioblastic grains (< 20 μm) and abundant
465 (Fig. 6-H). Titanite grains show no BSE zoning. Hematite is found as a product of sulphide
466 oxidation. Titanite grains in C147 are in clear equilibrium with the mineral assemblage at
467 lawsonite eclogite facies conditions. This contrasts with the Monviso eclogites, where rutile is
468 the HP stable Ti-phase and occasionally titanite is only found as a retrograde phase (PG).

469 **3.2. TiO_2 polymorphism**

470 IODP and Chenaillet samples yielding what was recognised petrographically as rutile were
471 subjected to an inspection using Raman spectroscopy to confirm the polymorphism. Grains
472 from 4 IODP samples (1316, 1319, 1320, and 5450) and from 3 Chenaillet samples (Ch1, Ch3
473 and ChDi) were analysed. The Raman spectrum for each of these measurements was
474 compared with spectra of rutile, anatase and brookite from the RRUF database (Figs. 7-9 in
475 Supplementary Data: Electronic Appendix 1). Without exception, for both coarser grains and
476 finer lamellae, rutile was always the TiO_2 mineral identified.

477 A summary of P-T conditions associated with stable Ti-phase in each sample, can be
478 found in Figure 7. The larger T range in the IODP and Chenaillet samples is related to the
479 uncertainty in the conditions of Ti-phase growth in those rocks.

480 **3.3. Ti-phase mineral chemistry**

481 3.3.1. *Titanite*

482 *Major and minor elements.*

Titanite from the Atlantic IODP samples (1316, 1319, 1320) shows lower X_{Al}, between 0.026 and 0.045, and F (F_{pfu} < 0.003), with respect to those of Chenaillet titanite, that yield X_{Al} between 0.066 and 0.077, and F_{pfu} between 0.003 and 0.007. On the other hand, titanite grains retrieved from the Indian IODP (5450) sample exhibit higher values, with X_{Al} of about 0.106 and F_{pfu} of about 0.026. Titanite formed at higher pressure, from the blueschist and eclogite metagabbros, are homogeneous with X_{Al} between 0.022 and 0.033 and low F concentrations with F_{pfu} < 0.005 (Fig. 8).

In a X_{Al} vs F_{pfu} diagram, published data of titanite chemistry from mafic eclogite, carbonate-rich eclogite, from UHP, HT calcsilicate, upper amphibolite calcsilicate, high-temperature marbles, felsic and mafic amphibolite rocks are also reported. The upper amphibolite calcsilicate rocks and the marbles present the highest X_{Al} and F_{pfu}. These are followed by the felsic upper amphibolite units and UHP-upper amphibolite calcsilicate titanite. Our data plot at slightly lower F pfu than the literature dataset reported in Figure 8. LT-HP metamorphic titanite show the lowest X_{Al} and can be separated from MT-LP metamorphic titanite in this dataset based on X_{Al} but not F pfu. It should be noted that titanite found in the granulite oceanic samples show the lowest F values (Fig. 8). The lack of mineral chemistry data from more mafic protolith titanite prevents a more robust comparison.

High Field Strength Elements, V and Sn.

Titanite grains from the IODP amphibole-bearing gabbros yield average Nb/Ta values around 16.8 ± 9 (Fig. 9a). This contrasts to the extreme, and variable Nb/Ta ratios in titanite grains from the pre-Alpine Chenaillet ophiolite (Ch3; Nb/Ta 16.2 – 208). The Chenaillet ophiolite seems to have been strongly affected by an ocean-floor, late-stage fluid circulation (*e.g.* Nicollet et al., 2022). Some titanite found in thin veins show increased Nb/Ta values in comparison to other titanite grains found in amphibole coronas (average Nb/Ta 128 vs 47,

507 respectively). However, even corona-related titanite in the Chenaillet yields higher Nb/Ta
508 values than titanite in IODP amphibole-bearing gabbros (Fig. 9a). Unlike Nb/Ta, Zr/Hf values
509 are less variable across all HT samples (Fig. 8a). For instance, Chenaillet titanite yields
510 average Zr/Hf of ca. 29 ± 11, in good agreement with Zr/Hf from IODP titanite (28 ± 15).
511 Finally, blueschist (QE-1, QE-6, TR10, C16) titanite grains yield average Nb/Ta 17.1 ± 13 (6
512 – 67) and Zr/Hf 19.8 ± 9 (9 – 45). Overall, the majority of titanite grains have average
513 chondritic Nb/Ta but lower than chondritic Zr/Hf values (Fig. 9a).

514 Figure 9b depicts our titanite data in a V vs Sn diagram (Xiao et al., 2020). The
515 majority of titanite grains yields Sn content < 40 ppm, irrespective of metamorphic grade, and
516 only a few titanite crystals (4 grains) show higher Sn content (40-100 ppm). Vanadium
517 compositions of all titanite are more variable and can go as high as 2500 ppm (Fig. 9b).
518 Titanite grains from MT-LP conditions show a wide range of Sn compositions: i) IODP1320
519 sample yield the lowest Sn and V values (< 10 and < 500 ppm, respectively), while ii)
520 IODP1319 and Ch3 yield higher Sn content (10 – 100 ppm) but similar V chemistry. In the
521 Queyras blueschist, Sn is within uncertainty of granulite-facies titanite grains but have
522 variable and higher V contents (up to 1500-2500 ppm). This is clearly at odds from titanite
523 grains from Corsica (LT eclogite) that yield narrower V (< 500 ppm) and Sn (10-30 ppm)
524 compositions (Fig. 9b).

525 *Yttrium, Rare Earth Elements and Th/U ratios.* In the metagabbros, titanite grains
526 yield highly variable Y and REE compositions, from more enriched to depleted, from strongly
527 fractionated to unfractionated (Fig. 10).

528 Titanite can incorporate significant amounts of Y (Scibiorski et al., 2019). LP titanite
529 yields two groups based on Y (Supplementary Data: Electronic Appendix 3), one yielding a
530 narrow concentration range (sample 1320: 1 – 252 ppm; and from Chenaillet Massif Ch3: 5 –

222 ppm), while the other shows more elevated and variable Y contents (samples 1316 and 1319: 152 to 4095 ppm). HP titanite (QE-6, TR10, and C16) range between 70 and 500 ppm Y content.

Titanite grains that form under LP conditions (Ch3 and IODP1319 amphibolites) show a wide range of REE contents (∑REE = 10 - 3350 ppm) and flat REE patterns (La/Yb_N = 0.02 – 1.67)(Fig. 10). Eu anomalies on these units are highly variable (Eu/Eu* = 0.22 – 29.5). Titanite grains from IODP1320 sample have a similar range of REE contents (∑REE = 12 – 2006 ppm), but show different chondrite-normalised REE patterns (Fig. 10), with LREE enriched patterns (La/Yb_N = 11 – 113), (La/Sm_N = 5 - 93) and clear positive Eu anomalies (Eu/Eu* = 4.7 – 314). Th/U ratios from all these LP rocks are commonly < 1.1 except for one outlier. They show either small scatter within sample (Ch3 and 1319 Th/U = 0.35 ± 0.1) or some variation (sample 1320; Th/U = 0.08 – 1.06).

Titanite grains retrieved from HP metagabbros and metabasalts show low REE contents (∑REE = 32 - 465 ppm), of which ∑LREE represent 4 to 210 ppm. Blueschist rocks from Queyras (QE-1, QE-6, TR10) show consistent depleted titanite LREE pattern (La/Sm_N = 0.02 – 0.7), similarly to eclogite rocks from Corsica (La/Sm_N = 0.02 – 0.3). Eu anomalies are non-existent to only slightly positive (Eu/Eu* = 0.84 – 1.8). Th/U ratios show small scatter within the HP samples, commonly < 0.4. These features are summarised in Table 3.

3.3.2. *Rutile*

Minor and trace element composition of rutile grains from two IODP gabbros, from eclogite and as inclusions within titanite from blueschist rocks are reported in Figure 11. Chromium and Nb contents are generally low (< 600 ppm), with only some rutile grains exhibiting more elevated Nb (800 - 1500 ppm) and Cr (800 - 1400 ppm) (Fig. 11a; IODP gabbros). In this way, almost all rutile plot in the *metamafic field* defined by Meinhold et al. (2008), and only a few IODP grains plot within the *metafelsic field*. In the diagram Zr/Hf vs Nb/Ta (Fig. 11b),

556 the majority of the analyses display Zr/Hf (20 – 40) and Nb/Ta (12 – 30) values in the
557 *metamorphic field* defined by Pereira et al. (2019). A limited number of rutile grains display
558 lower ratios, typical of rutile precipitated from hydrothermal-related fluids (Fig. 11b), that
559 plot within the metamafic in Figure 11a.

560 A ternary diagram constructed using V+Cr, Sc and Nb as endmembers to explore the
561 variance in our dataset (as determined by a PCA analysis) is presented in Figure 11c. Rutile
562 grains from eclogite plot in a field closer to higher V and Cr, unlike rutile grains that formed
563 under LP conditions (IODP gabbros or inclusions in blueschist titanite; Fig. 11c). The latter
564 plots closer to Sc, while the former has variable Sc-Nb. In Figure 10d we present the sum of
565 the HFSE ratios against the Nb/V ratio. Rutile in eclogite display high ∑Zr/Hf, Nb/Ta (>25)
566 and low Nb/V (<0.3), while low pressure granulite to upper amphibolite rutile show higher
567 Nb/V (>0.3). Using previously defined fields shown in Figure 11b, rutile grains with low
568 ∑Zr/Hf, Nb/Ta (<25) are likely related to fluid precipitation processes (Pereira et al., 2019).

569 As shown in section 3.1, ilmenite in amphibole-bearing gabbros (IODP) often display
570 partial replacement by titanite and rutile. These are also the samples where rutile chemistry is
571 less homogeneous. In these composite grains, rutile is found such as the grain depicted in
572 Figure 12, either as very fine lamellae, frequently displaying 120º/60º intersections, or as
573 coarser grains, mostly frequently rimmed by titanite (example spot 4 and 9* in Fig 12a), but
574 also just by ilmenite (example spot 7 in Fig 12a).

575 A diagram of Cr against Zr values is shown in Figure 12b, where two distinct rutile
576 groups are highlighted: (i) grains that are low in Cr (< 600 ppm) and low in Zr (< 300 ppm),
577 and (ii) grains with Cr content above 600 ppm with higher Zr content (500-2500 ppm). The
578 most enriched analysis (7 in Fig. 11) corresponds to a rutile grain surrounded by ilmenite as
579 an inclusion (Fig 12a). The analyses with the lowest Zr, Cr, and V are fine-grained rutile,

580 commonly closer to the former edges of the ilmenite grain (Fig 12a, spots 10, 11, 12, and 1).
581 Yet, the relation between the enrichment in Cr-Nb-Zr and the rutile textural position within
582 the composite grain (lamellae or inclusion) is not perfectly systematic.

583 3.3.3. *Ilmenite*

584 The chemical composition of ilmenite was investigated using EPMA and LA-ICP-MS,
585 focusing on two samples from the IODP drill cores, 1320 and 5450, which contained the
586 largest ilmenite grains. These ilmenite grains yield variable Fe_2O_3 (4.7 and 17.6 wt%) and
587 MgO (12.6 and 4.7 wt%) compositions, similar MnO (0.22 and 0.25 wt%) and TiO_2 (3.3 and
588 4.9 wt%) and overall low Al_2O_3 (120 to 365 ppm). In sample 1320 (higher bulk Al and Mg),
589 ilmenite incorporates more Al (341 ppm) and Mg (4.1 wt%) than in sample 5450 (Al 134 ppm
590 and Mg 0.5 wt%). A small variation in WR MnO abundance ($\Delta \sim 0.03$ wt%) seems to reflect
591 highly on Mn incorporation into ilmenite (4 369 to 8 289 ppm; Supplementary data:
592 Electronic Appendix 2).

593 To investigate WR dependency of trace elements in ilmenite, we use Al against other
594 trace elements (Mn yields similar results; Fig 13). Vanadium and Zr inversely correlate with
595 Al, while Cr correlates positively. This seems to imply that at higher Al_2O_3 compositions in a
596 gabbro, ilmenite incorporates less V and Zr (Fig. 13). Conversely, more Cr will be
597 incorporated by ilmenite in a more enriched Al_2O_3 composition. Incorporation of Yb, Nb and
598 Ta by ilmenite does not correlate with Al (nor Mn). Particularly for one sample (IODP1320;
599 Fig. 13) there is either clustering (Yb and Ta) or scatter (Nb) for similar Al values in ilmenite
600 and for the same bulk Al_2O_3. This can indicate the presence of two distinct ilmenite
601 populations.

4. DISCUSSION

4.1 Ti-phase stability: from oceanisation to subduction

4.1.1 *Ti-minerals in ocean floor amphibole-bearing gabbros (LP-MHT)*

Our data show that ilmenite, titanite, and rutile are present at very low-pressure, and moderate to high temperature (amphibolite to granulite) conditions in the oceanic crust. Their formation history can be deduced from their petrographic textures and chemical signatures. Ilmenite can be a product of magmatic and/or later metamorphic recrystallisation, as it commonly forms the core of ilmenite-titanite composite grains. Fine rutile-titanite lamellae showing 120°/60° angles indicate an exsolution of excess Ti during titanite overgrowth on ilmenite at lower grade. Rutile found as coarser grains (10-40 µm; *e.g.* sample IODP1316) is more puzzling. At times, coarse rutile is found with no ilmenite surrounded by a titanite corona (*e.g.* IODP1316), while other rutile grains are found surrounded/intergrown by/with ilmenite and then by a titanite corona (IODP1320; Fig. 3). The former is suggestive of an earlier origin of rutile in the gabbro, either HT metamorphic or a late-stage magmatic crystallisation related to fluctuations in the magma fO_2 (Toplis and Carroll, 1995) enhanced by fluid/melt percolation (Tribuzio *et al.*, 2000). While texturally these could be envisaged as magmatic, this would require magmas with elevated TiO_2 (7-10 wt%; Ryerson and Watson, 1987), such as in more fractionated magmas in the oceanic crust (Whitaker *et al.*, 2007). The second is more difficult to interpret, as rutile can be potentially coeval with ilmenite recrystallisation or interpreted as an earlier phase. Rutile (lamellae, coarse grain) found in IODP samples, can also be tentatively distinguished by their chemistry: one group exhibits slightly higher Nb-Zr-Cr compositions, potentially formed at higher temperatures than the other group that yields lower Nb-Zr-Cr, corresponding strictly to the fine lamellae formed during titanite-rutile replacement of ilmenite (Fig.12). This replacement process generally takes place at amphibolite-facies

conditions (ca. low temperature ~600 ºC). At such temperature, amphibole does not incorporate Ti released by ilmenite breakdown, and thus rutile forms within titanite.

Titanite in the IODP and Chenaillet metagabbros is texturally associated with the breakdown of brown to green amphibole, or occurs as replacement textures after ilmenite, under amphibolite facies conditions. A rare third type of titanite exhibiting strong chemical zoning (Fig. 4-H), formed at a later stage during fluid percolation associated with actinolite at greenschist facies cooling conditions, is well documented in Ch1 – Chenaillet ophiolite (Nicollet et al., 2022).

In summary, Ti-phases in oceanic gabbros evolve from magmatic ilmenite at HT conditions to low temperature titanite by hydrothermal metamorphism during cooling, while rutile potentially crystallise during early and late ocean floor metamorphism due to local or global Ti excess.

4.1.2 *Ti-phase stabilities in the subducting slab*

As the oceanic crust undergoes subduction, new minerals stabilise to higher pressures and temperatures. Here, metagabbros from the Queyras-Monviso and Corsica preserve mineral assemblages equilibrated at blueschist and eclogite facies conditions. Overall, titanite appears stable at LT-HP, except in eclogite samples from Monviso. Typically, titanite grains are found in equilibrium with lawsonite in the Queyras blueschist and Corsica eclogite. They have small grain sizes and are idioblastic in the metabasalt (Fig. 6), while often xenoblastic (Fig. 5) or in small aggregates (Fig. 5) in the metagabbros. Occasionally in the blueschist from Queyras (metagabbros), titanite shows porous texture, with frequent but very small rutile grains. We interpret these as inclusions, as they only occur in the cores of larger titanite and never where titanite grains are fine-grained, and thus better equilibrated. These inclusions are often lamellar, with the preserved 120°/60° angles. These textures are very similar to those found in the oceanic metagabbros. No ilmenite is found in these titanite grains. These textures are

suggestive of rutile being a relic phase (such as magmatic clinopyroxene in the same rocks) preserved within the recrystallised titanite grains, as testimonies of the ocean-floor metamorphic evolution.

Rutile is stable in Monviso eclogite and titanite is absent, except for retrograde titanite rimming rutile in the Passo Gallarino eclogite. At similar P-T conditions, titanite is found stable together with lawsonite and omphacite in Corsica samples and rutile is found stable with garnet, omphacite and zoisite in Monviso. A study has argued that titanite reacts to form rutile tied with lawsonite disappearance to form epidote (Frost *et al.*, 2001), which potentially could explain the differences between these eclogite samples.

Lawsonite and titanite stabilities. The Corsican lawsonite eclogite is one of the few occurrences reported in the literature where titanite is found in equilibrium at eclogite facies (*e.g.* Vitale-Brovarone et al., 2011; Sassi *et al.*, 2000; Ng *et al.*, 2016). Frost et al. (2001) explains that the dehydration reaction of lawsonite producing zoisite and quartz leads to titanite breakdown and rutile formation, as zoisite incorporates more Ca than lawsonite. In detail, this reaction is sensitive to water activity (Clarke et al., 2006), bulk composition (Davis and Whitney, 2006, SiO_2-Al_2O_3) and CO_2 in fluids (Castelli and Rubatto, 2002). Previous authors showed that this reaction yields a positive Clapeyron slope, taking place at higher pressure with increased temperature, until about 500 to 600 °C, and then it becomes mainly temperature-dependent (Clarke *et al.*, 2006; Whitney and Davis, 2006). Perhaps as a consequence, there have been few reported occurrences of rutile stable with lawsonite under blueschist or eclogite conditions (*e.g.* Bianco *et al.*, 2019 in the Elba Island – Italy, Maruyama et al., 1998 in the Franciscan Complex – USA, and Groppo and Castelli, 2010 in Monviso - W. Alps). This implies that while the net-reactions might influence what components are available to stabilise titanite or rutile, rutile can appear while lawsonite is yet stable, and

675 therefore the transition between HP titanite to rutile is an interplay with other factors such as
676 major oxides, H_2O, and/or CO_2.

677 4.1.3 *The effects of MORB whole rock composition on titanite and rutile stabilities*

678 It has been well established that for rocks with MORB composition, rutile is more stable at
679 high pressure conditions, while titanite and ilmenite at lower pressures, with ilmenite more
680 stable than titanite at higher temperatures (e.g. Liou et al., 1998). Yet, due to natural
681 exceptions to these phase relationships, in the following we explore other factors that play a
682 role in their stability, with a special focus on bulk rock chemistry. The stability of rutile, for
683 example, is mostly influenced by the bulk TiO_2 concentration, whereas titanite is more
684 sensitive to variations in overall bulk geochemistry (Frost et al., 2001; Angiboust and Harlov,
685 2017). In Ca-rich protoliths, the following reactions maximise titanite stability: rutile +
686 grossular + diopside ↔ pyrope + titanite (1) and rutile + quartz + calcite ↔ titanite + CO_2 (2)
687 (Spear, 1993). The presence of carbonate minerals favour titanite (Cave *et al.*, 2015). The
688 water activity at HP is also an important parameter, as H_2O will favour hydrous minerals and
689 thus titanite as indicated by the following reaction: lawsonite + titanite ↔ zoisite + rutile +
690 quartz + H_2O (3) (Frost *et al.*, 2001). Indeed, the Corsican eclogite is richer in H_2O than the
691 Monviso eclogite (Supplementary Data: Appendix 1), where one yields titanite and the other
692 rutile. Yet, as also seen in reaction (2), CO_2-rich fluids favour rutile instead of titanite. It has
693 also been shown that the F-Al coupled substitutions seems to stabilise titanite above its
694 commonly known stability conditions, more so in Ca-rich protoliths (marbles), at HT or HP
695 (Castelli and Rubatto, 2002; Tropper *et al.*, 2002; Fig. 8). While titanite tends to disappear
696 with increasing SiO_2 (Frost *et al.*, 2001), this is mostly linked to the concurring decrease of
697 CaO. Thus, it has long been established that the Ca/Al ratio is key in the stabilisation of
698 titanite (Frost *et al.*, 2001). Reflecting on the considerations above, the presence or absence of
699 Ti-phases are shown in a plot comparing Ti/Ca and Ca/Al bulk rock values, using data from

700 our LT-HP samples combined with Syros HP rocks, and average MORB published data (Fig.
701 14). Ti/Ca values are expected to influence rutile stability while Ca/Al should mostly
702 influence titanite stability as it competes with plagioclase, lawsonite or epidote. With
703 increasing Ca/Al, even at elevated Ti/Ca, we expect titanite to be stable, leading to a field
704 where both rutile and titanite should be stable (Ca/Al values above ~ 0.85). It should be noted
705 that the compositional range of this set of rocks is limited: bulk SiO_2 (46-51 wt%) and CaO
706 (9-14 wt%), and TiO_2 ranges from 0.25 to 3.17 wt% (Supplementary Data: Electronic
707 Appendix 1 – Table 5) and that no calcite was observed or reported.

708 Several conclusions can be drawn from the figure:

709 – Blueschist and eclogite rocks with stable titanite yield variable Ca/Al (commonly higher
710 than 0.75) while Ti/Ca is systematically below 0.15. On the contrary, blueschist and
711 eclogite with stable rutile exhibit Ti/Ca values above 0.15. These data seem to support the
712 major control of reaction (1) on rutile and titanite stability at LT-HP conditions. This is
713 consistent with data on blueschist and eclogite from Syros (Marschall 2005) for which
714 rutile-bearing HP units plot in the Ti/Ca > 0.15 field.
715 – Unaltered MORB values yield relatively low Ti/Ca values (0.05 - 0.15) and variable but
716 high Ca/Al that range from 0.8 to 1.2 (Fig. 14; Klein, 2004). These compositions at low
717 geothermal gradients favour titanite over rutile growth. However, a relative increase of Ti
718 and Fe in respect to the other major elements is expected for the altered oceanic crust
719 metamorphosed by either hydrothermal or seawater fluid interactions (Staudigel and Hart,
720 1983). Al-saponite type alteration of Fe-bearing minerals (e.g, oxides and
721 clinopyroxenes) and albitisation of primary plagioclase can also lead to considerable Ca-
722 loss (Alt *et al.*, 1992), and thus alteration of MORB rocks are likely to increase Ti/Ca and
723 variably decrease Ca/Al values.

4.2. Controls on Ti-bearing mineral chemistry

4.2.1. Ilmenite trace element compositions: bulk-rock effect

Our limited data show that ilmenite major and minor element compositions are strongly dependent on bulk-rock composition. The binary plots of Al against multiple trace element contents in ilmenite illustrate how Cr seems to be positively correlated with Al, which in turn correlates with the Al_2O_3 content of the metagabbros (Fig. 13). Niobium and Ta showed no significant correlation with Al, indicating the presence of two chemically distinct ilmenite populations in each sample. This implies that other factors are more relevant in the intake of Nb and Ta by ilmenite, such as competition with rutile (*e.g.*, sample 1320).

4.2.2. Titanite trace element compositions: the role of fluids and HREE-bearing minerals

Titanite from LP settings. Titanite from our dataset show Nb/Ta values that are within uncertainty of the chondritic value (Fig. 9a; McDonough and Sun, 1995), except a few titanite from the Chenaillet Massif amphibolite metagabbro that yield Nb/Ta > 100 (Fig. 9a). Titanite Zr/Hf values, on the other hand, are persistently subchondritic. The high-field strength elements (HFSE) pairs, Zr and Hf, and Nb and Ta have a degree of geochemical affinity that prevents their fractionation under most geological conditions. However, some fractionation between each pair in metamorphic titanite has previously been reported (Chen and Zheng, 2015). Cherniak (2015) has constrained the diffusivities of these elements in titanite and her data suggest that unlike in rutile, diffusive fractionation should not be a likely mechanism to explain variable titanite Nb/Ta ratios. Therefore, fractionation between these elements in titanite is promoted by other processes such as growth in the presence of external fluids or after the break down of minerals with variable compatibility with these elements. In this way, we interpret these higher to extreme Nb/Ta values found in the Chenaillet Massif to be derived from external fluids related with differentiation of the lower oceanic crust, during cooling. Additionally, some of the Chenaillet Massif titanite grains (Ch3) can also yield

749 higher Sn (> 60 ppm; Fig. 9b). Elements like Sn and Mo are usually associated with titanite
750 growth from hydrothermal fluids (such as in Fu et al., 2016). This may support the existence
751 of externally derived late-stage fluids during titanite growth. These data are compatible with
752 the late-stage texture of titanite in these rocks, associated with brown to green amphibole
753 breakdown and alteration of former ilmenite grains.

754 *Y-REE behaviour*. Titanite mineral chemistry has been heavily addressed over the
755 years, as its chemistry seems to be a faithful recorder of petrogenetic processes (Bruand *et al.*,
756 2014, 2016; Scibiorski *et al.*, 2019). Titanite incorporates a significant amount of REE and Y,
757 of which Y and HREE are also incorporated by major mineral garnet. Scibiorski et al. (2019)
758 have demonstrated how titanite growing in competition with garnet, in garnet amphibolites
759 and gneisses (both felsic and intermediate), is significantly affected in key HREE. In their
760 study, they demonstrated that by using Y vs Dy/Yb titanite grown in garnet-absent rocks can
761 be distinguished from garnet-bearing rocks. We have plotted titanite data from our study in
762 the same diagrams (Fig. 15). Except for the Corsica eclogite, all our titanite-bearing samples
763 are garnet-free. Commonly Y substitutes with HREE and thus there is a linear correlation
764 between HREE and Y values (Fig. 15a). Titanite grains retrieved from Corsica eclogite-facies
765 rocks have a different Y/HREE slope than titanite from the other units (Fig. 15a). While in the
766 original study by Scibiorski et al. (2019), Dy/Yb faithfully discriminated titanite of garnet-
767 bearing from garnet-free domains, some of our titanite from garnet-absent units (e.g. Ch3)
768 yield high Dy/Yb (> 2.0; Fig. 15b). This suggests that i) there is competition with another
769 mineral for Yb, such as zircon and/or xenotime, ii) that titanite might incorporate more Dy
770 due to break down of a main phase that favours MREE such as zoisite (Frei et al., 2004) or iii)
771 that at HP-LT conditions, Yb partition coefficient in titanite changes.

4.2.3. Rutile trace element compositions: Cr and High Field Strength Elements

Cr-Nb discrimination diagram. Rutile from our dataset (n=69) are derived from metagabbros (mafic). We applied the Cr-Nb protolith discrimination diagram from Meinhold *et al.* (2008) and while the majority of rutile plot in the metamafic field, there are 7 grains classified as metafelsic-derived. These correspond to grains retrieved from the IODP amphibole-bearing gabbros (samples 1316 and 1320). These results confirm that rutile derived from high-grade conditions can be misidentified using this discrimination tool, such as highlighted by Meinhold *et al.* (2008). This suggests that at high-grade conditions, Cr is not always preferentially retained by rutile, as Cr is more diffusive than Nb at HT (Sasaki et al., 1985; Marschall et al., 2013) or as a new source of Nb becomes available (*e.g.* amphibole or ilmenite breakdown). This seems to be the case, due to the incongruent replacement of ilmenite in the ilmenite-titanite-rutile aggregates. It is not fully clear whether rutile and ilmenite are initially stable together, as textural relationships seem to suggest, and thus competing for Nb. No evidence of HT amphibole breakdown was identified in sample 1320, and this can explain Cr being sequestered by either HT amphibole or by primary clinopyroxene (such as in Tribuzio *et al.*, 2019).

High Field Strength Elemental ratios. Zr/Hf and Nb/Ta values from rutile plot within known compositions of other metamorphic rutile, except for 4 grains that have ∑Nb/Ta, Zr/Hf < 25, which plot within the fluid-related rutile field of Pereira *et al.* (2019). These grains come from sample IODP1319, a LP amphibolite, where rutile occurs as spherical inclusions always surrounded by ilmenite. As discussed in the previous section, these rutile grains seem to reflect a higher temperature growth, in respect with the fine rutile lamellae, as they occur as inclusions in ilmenite. Yet, these grains yield the lowest values for several trace elements within the IODP dataset (Cr < 11, Zr < 204, Nb < 450 ppm). This might imply that these

grains have strongly fractionated Nb/Ta and Zr/Hf values, typical of LT-LP rutile. The low Zr/Hf values (7.22 - 13.66) are consistent with rutile formed at LT (Ewing *et al.*, 2014).

4.3. Are titanite and rutile chemistries pressure and temperature sensitive?

4.3.1. Titanite

We filtered our titanite chemical data using Principal Component Analysis. This allowed to select certain trace elements that better explain the variance in the dataset, and plot them in a Yb, V+Cr and Nb+Ta ternary diagram (Fig. 16). Titanite grains from our LP oceanic amphibole-bearing gabbros plot closer to the Nb+Ta endmember, while titanite belonging to the HP assemblage from HP metagabbros plot between theYb and the V+Cr endmembers (Fig. 16a). Similarly, La/Sm, V and Yb allow to distinguish LP from HP titanite, as HP titanite are strongly depleted in LREE relatively to the MREE (Fig. 16c). To test these systematics, we compiled titanite trace element data from igneous rocks, gneisses (ortho-mafic and intermediate, and calc-rich), and HP-LT rocks from the literature (Fig. 16b, d).

Nb+Ta vs Yb. Igneous-related titanite (either more mafic or more felsic) is clearly distinguishable from other titanite and plot closer to the Nb+Ta apex in the ternary diagram (Fig. 16b). HT metamorphic titanite grains show similar behaviour, despite some outliers in the garnet amphibolite that tend towards the Cr+V endmember. Blueschist-derived titanite from the literature plot mostly in the centre of the diagram and tend to the Yb endmember (Nb = 10 to 30 ppm; Yb = 15 to 40 ppm) and are easily distinguished from the remaining titanite (igneous and HT). Yet, a few eclogite titanite grains from our study and other blueschist titanite (New Caledonia) plot closer to the Nb+Ta endmember (Fig. 16b). This implies that another mechanism is accountable for those titanite compositions. Eclogite from Corsica are often garnet bearing (C147), and therefore those titanite were in competition for HREE, explaining their lower Yb. The New Caledonia titanite form in garnet-free, metamafic and metapelitic blueschist (Spandler et al., 2003) and thus another explanation is required for their

Yb depletion when compared with the other blueschist-related titanite grains (8 to 30 ppm vs 20 to 50 ppm, respectively). There may be: i) competition for Yb with other minerals (such as apatite and lawsonite; Spandler et al., 2003), scavenging it before titanite growth, or ii) a relatively low Yb bulk composition (Spandler et al., 2003). In summary, although a ternary diagram such as presented in Fig.16b discriminate a large part of our LT-HP titanite dataset from other titanite, this diagram fails to discriminate all LT-HP reported in this figure and therefore a few other competing factors can influence these trace-elements distribution into titanite.

V content in HP titanite. Some titanite grains in our dataset show significant V contents (> 500 ppm), markedly in blueschist titanite from the Queyras. Minerals like pargasite, phengite, omphacite or epidote are major carriers of V. Indeed, titanite growth after biotite or hornblende breakdown has been shown to be more enriched in V (Xiao *et al.*, 2020). Blueschist from Queyras are predominantly lawsonite and glaucophane bearing, minerals that do not particularly favour V incorporation (Spandler *et al.*, 2003). This might explain why V is more incorporated by titanite in these samples. Conversely, in Corsica samples, titanite is equilibrated with omphacite who disputes more with titanite for V (Hermann, 2002; Spandler *et al.*, 2003). This seems to suggest that in the absence of omphacite or phengite, HP titanite grains can yield higher V contents, but the role of fO_2 should also be considered as V is redox sensitive.

REE contents, and the La/Sm vs Yb vs V ternary. It must be noted that on average, REE contents of igneous titanite are high, particularly for the LREE (Xiao *et al.*, 2014; Bruand *et al.*, 2020; Scibiorski and Cawood, 2022) and therefore these can be used as a first approach to distinguish igneous from metamorphic titanite. Titanite from our LP amphibolite facies samples go from depleted to mildly enriched REE, with no significant REE fractionation patterns. On the other hand, LT-HP blueschist and eclogite titanite grains show

strong depletion in REE and more particularly in LREE, which results in La/Sm_N fractionation and in negative slopes of the LREE pattern (Fig. 10). Lanthanum is mostly taken by lawsonite and epidote in mafic blueschist, and by apatite in more pelitic compositions (Spandler *et al.*, 2003; Martin *et al.*, 2014). However, epidote does not intake Sm (Spandler et al., 2003). This implies that epidote can lead to variable La and Sm availability and thus fractionation of these REE. We have thus used La/Sm_N against Yb (HREE) to investigate their potential as pressure discriminants applied to titanite from our study (Fig. 16c). Alpine HP units plot at lower La/Sm_N values and spread in between Yb and V endmembers. This is in sharp contrast with titanite grains from igneous and lower amphibolite conditions that tend to display no to small La/Sm_N fractionation and therefore plot close to the La/Sm_N apex (Fig. 16d). By applying a multiple-step discrimination approach, resourcing to the two ternary diagrams (Fig. 16b and d), different titanite types formed at variable settings and grades can be distinguished.

4.3.2. Rutile

Previously, we showed that the variability in our rutile dataset can be best described using V+Cr, Sc, and Nb endmembers in a ternary diagram (Fig. 11c). Based on this diagram, rutile from eclogite can be distinguished from amphibolitic-granulitic rutile. Available rutile data from the literature are also reported in two diagrams (Fig. 17). Despite the limited amount of mafic rutile data available from the literature reporting Sc, data from the literature agree well with the defined fields from this study. HP rutile from Syros and from a talc eclogite from Monviso plot together with eclogite rutile from our study in the HP field, whilst rutile from a mafic granulite plot together with LP rutile from our study in the newly defined LP fields of both diagrams (Fig. 17). Some rutile grains from the talc eclogite reported by Angiboust *et al.* (2014) are partially overlapping with some HT rutile in the 0.3-0.5 Nb/V range (Fig. 17b). Yet, the overall reproducibility of this diagram seems to sustain.

While only mafic-derived rutile were used here to test trace-element pressure dependency, there are however subtle compositional variations within gabbros and basalts from the ocean floor that can lead to variable rutile compositions. Due to the lack of available bulk trace element compositions for the set of rocks used in this study, we have, alternatively, tested the influence of composition by forward modelling trace element re-distribution in rutile using RStudio®. We have resourced to a compilation of trace element abundances from MORB and ophiolite gabbros (including some in our collection), and selected the elements of interest (V, Sc, Nb). We used parageneses and a range of mineral proportions like those found in our samples for both eclogitic (HP) and granulitic (HT) conditions, and published partitioning coefficients for all the mineral pairs considered. Details on the modelling parameters, inputs and outputs (ternary diagrams) are presented in the Supplementary Data: Electronic Appendix 5 and the script is available as Appendix 6. Even though generous uncertainties are incorporated into the forward model, as a reflection of large uncertainties in the mineral partitioning coefficients and phase proportions, rutile compositions of eclogite and granulite are always clearly separated, showing that this dichotomy is not primarily a function of bulk-rock geochemistry. The eclogite to granulite split occurs along the line parallel to the Sc-Nb join, as seen with our natural rutile data (Fig. 11c), indicating significant differences in the fractionation of V. Given that rutile-pyroxene partition coefficients differ only within a factor of two or so (Holycross and Cottrell, 2022), it appears that V distribution is controlled by major mineral assemblages which are clearly different between eclogite and granulite. It suggests that variations towards Nb are mainly controlled by the fraction of rutile in the rock, and the smaller the rutile fraction is, Nb in rutile increases.

What can explain V and Sc pressure dependency in rutile? Metamorphic rutile formed from mafic protoliths is commonly enriched in V (> 1000 ppm; Miller *et al.*, 2007; Gao *et al.*, 2010; Hart *et al.*, 2016). In our dataset, HP rutile plot systematically closer to the Cr+V

endmember when compared to the HT rutile. Vanadium is generally compatible with rutile, although at times it behaves as incompatible ($D_V^{Rutile/melt}$ 0.1 – 18, Klemme et al., 2005; $D_V^{Rutile/melt}$ 47 – 124, Foley et al., 2000). It has been demonstrated that V partitioning to rutile increases with increasing fO_2 (Holycross and Cottrell, 2020). This implies that V will be easily incorporated by rutile under most oxidising geological conditions. At higher temperature conditions, V might be preferentially incorporated into other phases (*e.g.* ilmenite, clinopyroxene, amphibole; Nehring *et al.*, 2010), and, as a consequence, rutile will contain less V and proportionally more Nb, for which it is the main carrier (Zack *et al.*, 2002). This seems to be the case of HT rutile grains that are plotted in Figure 17. The modelling also highlighted that V incorporation by rutile can also be controlled by bulk composition. Thus, V in rutile is controlled both by the element concentration, fO_2 and the paragenesis. As a result, if the compositional system is homogeneous (MORB), the critical factors are oxygen fugacity and minerals in competition with rutile.

Although rutile is commonly poor in Sc, Sc can behave similarly to Sb. Sc is often retained by amphiboles (e.g. glaucophane, pargasite), garnet or clinopyroxene in metabasites (Hermann, 2002; Spandler et al., 2003). Some Sc can be partitioned into rutile due to amphibole or primary Ti-rich clinopyroxene breakdown. This could account for some variable Sc found in rutile from the IODP and as inclusions in the Queyras titanite grains. As the modelling highlighted, the interplay of partitioning coefficients between the different clinopyroxenes (omphacite and augite) and hornblende exerts a strong control on Sc contents in rutile.

4.4. Applications and future directions using Ti-bearing minerals for LT-HP hunting

As we probe the exposed and preserved metamorphic rock record through time, retrieving HP metamorphic conditions before the Neoproterozoic has been challenging (e.g., Brown and Johnson, 2018; Palin *et al.*, 2020). There seems to exist a preferential preservation of HT

orogenic cores in ancient mountain belts (*e.g. Hercynian Massif Central*). The scarcity or absence of HP metamorphic rocks in ancient metamorphic belts can potentially be explained by a low preservation potential and, therefore, detrital grains formed after weathering of those units may be their only survivors. Rutile and titanite are easily found as detrital grains in stream sediments and in sedimentary rocks (*e.g.* Pereira *et al.*, 2020; Zhou *et al.*, 2020) but P-dependent proxies are required to discriminate HP from LP metamorphic rutile and titanite. In this contribution we have presented data of mafic rocks that underwent metamorphism both in the ocean floor, at low pressure, and during subduction at higher pressures. Our data suggest that Nb/V and Sc-Nb-V+Cr in rutile and V-Yb-La/Sm in titanite are pressure dependent (Figs. 16-17). To apply these petro-geochemical tools in sediments, we propose a multi-step discrimination approach, explained in the following.

For titanite, a first approach is to examine BSE images to select igneous from metamorphic titanite based on BSE zoning (Bruand et al., 2014 for magmatic; Garber et al., 2017 for metamorphic). Grains showing no zoning or metamorphic zoning can be selected and their trace element data plotted on the ternary diagrams proposed here (Fig. 16-b,d). This discrimination, however, leads to some HP titanite potentially being discriminated as LP.

For rutile, data should be plotted in diagrams that discriminate metamorphic derived from other rutile types (Agangi *et al.*, 2019; Pereira *et al.*, 2019). A sub-selection of metamorphic-only rutile can then be plotted using the Cr-Nb discriminating diagram (Meinhold et al., 2008 and others) to pool metamafic-derived rutile grains. This subset can then be projected in the Sc-Nb-V+Cr and Nb/V vs ∑Zr/Hf, Nb/Ta diagrams (Fig. 17). Further work is required to assess suitability for rutile grains derived from metapelitic protoliths.

5. Conclusions

In this study we have compared metamafic rocks with MORB affinities of modern and pre-alpine oceanic crust (IODP and Chenaillet massif) to metagabbros and metabasalts that have undergone HP during subduction to the blueschist and eclogite facies conditions (Queyras, Monviso, Corsica).

Despite rutile being mostly recognised as a stable phase at eclogite and upper amphibolite/granulite conditions due to Barrovian metamorphism, we found that amphibole-bearing gabbros in the oceanic crust can stabilise rutile at HT and very LP (ca. 2 kbar) (Fig. 18). Pressure and temperature are among the most critical parameters affecting the stability of these two minerals. Yet, we show that for rocks that experienced similar P-T conditions, subtle variations in the Ti/Ca and Ca/Al values seem to affect the titanite to rutile formation, even in rocks with similar bulk chemistry and grain sizes. These ratios, which may shift locally during mineral replacement reactions, can be the main controlling factor when both rutile and titanite are found stable at either LP or HP, especially in only partially equilibrated metagabbros.

Trace-element based discrimination tools are complex, and the chemistry of mineral phases are dependent on several factors including the bulk rock composition, local equilibria, partitioning coefficients between minerals and rocks and co-existing mineral phases during Ti-phase growth. Our results highlight that titanite trace element compositions in different MORB affinity metamafic rocks show strong variability. Titanite from our study shows that blueschist and eclogite yield a marked La depletion, and thus low La/Sm_N values in comparison to amphibolite grade titanite. La/Sm_N or Nb+Ta together with Yb and V can be used to discriminate HP titanite. Rutile grains from the metagabbros studied here display distinctive chemistries that are pressure indicative; rutile from HT-LP yield V/Nb values above 0.5 while V/Nb in rutile from eclogite facies are below 0.3. In the same way, V+Cr, Sc,

and Nb compositions can be used, following the workflow described in the discussion, to distinguish HP from LP metamafic rutile.

Acknowledgments

The authors thank the IODP for the access to the core samples used in this manuscript (request number 23095A). We would like to thank Jean-Luc Devidal for continuing support in the EPMA and LA-ICP-MS lab facilities at the LMV. This work was supported by the French Government Laboratory of Excellence initiative n° ANR-10-LABX-0006. This is Laboratory of Excellence ClerVolc contribution number XXX. This work is part of a project that has received funding from the European Research Council (ERC) under the European Union's Horizon 2020 research and innovation programme (Grant agreement No. 864045).

Data Availability Statement

The data underlying this article are available in the article and in its online supplementary material.

Supplementary Materials are available in the electronic version online. Appendix 1 comprises a full method description, sampling details, amphibole mineral chemistry detailed description and phase diagram modelling details. Appendix 2 includes silicate mineral chemistry and amphibole thermometry. Appendix 3 includes the full titanite, rutile and ilmenite chemistry dataset.

References

Abe, N. (2011). Petrology of podiform chromitite from the ocean floor at the 15°20′N FZ in the MAR, Site 1271, ODP Leg 209. *Journal of Mineralogical and Petrological Sciences* **106**, 97–102.

Agangi, A., Reddy, S. M., Plavsa, D., Fougerouse, D., Clark, C., Roberts, M. & Johnson, T. E. (2019). Antimony in rutile as a pathfinder for orogenic gold deposits. *Ore Geology*

992 *Reviews*. Elsevier **106**, 1–11.

993 Agard, P., Jolivet, L. & Goffé, B. (2001). Tectonometamorphic evolution of the Schiste
994 Lustrés complex: implications for the exhumation of HP and UHP rocks in the western
995 Alps. *Bulletin de la Societé Geologique de France* **172**, 617–636.

996 Alt, J. C., France-lanord, C., Floyd, P. a, Castillo, P. & Galy, A. (1992). Low-temperature
997 hydrothermal alteration of Jurassic ocean crust, Site 801 saponite-type alteration
998 alteration types and distribution. *Proceedings of the Ocean Drilling Program, Scientific*
999 *Results* **129**, 415–427.

1000 Angiboust, S. & Glodny, J. (2020). Lithos Exhumation of eclogitic ophiolitic nappes in the W
1001 . Alps : New age data and implications for crustal wedge dynamics. *LITHOS*. Elsevier
1002 B.V. **356**–**357**, 105374.

1003 Angiboust, S., Pettke, T., Hoog, J. A. N. C. M. D. E., Caron, B. & Oncken, O. (2014).
1004 Channelized Fluid Flow and Eclogite-facies Metasomatism along the Subduction Shear
1005 Zone. **55**, 883–916.

1006 Ashley, K. T., Caddick, M. J., Steele-Macinnis, M. J., Bodnar, R. J. & Dragovic, B. (2014).
1007 Geothermobarometric history of subduction recorded by quartz inclusions in garnet.
1008 *Geochemistry, Geophysics, Geosystems* **15**, 350–360.

1009 BALLEVRE, M., Lagabrielle, Y. & MERLE, O. (1990). Tertiary ductile normal faulting as a
1010 consequence of lithospheric stacking in the western Alps. *Mémoires de la Société*
1011 *géologique de France (1833)* **156**, 227–236.

1012 Batiza, R. & Vanko, D. A. (1985). Petrologic evolution of large failed rifts in the Eastern
1013 Pacific: Petrology of volcanic and plutonic rocks from the mathematician ridge area and
1014 the guadalupe trough. *Journal of Petrology* **26**, 564–602.

1015 Bianco, C., Godard, G., Halton, A., Brogi, A., Liotta, D. & Caggianelli, A. (2019). The
1016 lawsonite-glaucophane blueschists of Elba Island (Italy). *Lithos*. Elsevier Ltd **348**–**349**,
1017 105198.

1018 Blackman, D. K. (2006). Proceedings of the Integrated Ocean Drilling Program, 304/305.
1019 *http://iodp. tamu. edu/publications/exp304_305/30405title. htm*. Integrated Ocean
1020 Drilling Program Management International, Inc.

1021 Blake, C. & Moore, D. G. (1995). The role of the serpentinite melange in the unroofing of the
1022 UHP rocks: an example from the western Alps in Italy." from Coleman RG and Wang
1023 X.(eds). Ultrahigh pressure metamorphism. Cambridge University Press.

1024 Brown, M. & Johnson, T. (2018). Secular change in metamorphism and the onset of global
1025 plate tectonics. *American Mineralogist* **103**, 181–196.

1026 Bruand, E., Fowler, M., Storey, C., Laurent, O., Antoine, C., Guitreau, M., Heilimo, E. &
1027 Nebel, O. (2020). Accessory mineral constraints on crustal evolution: elemental
1028 fingerprints for magma discrimination. *Geochemical Perspectives Letters* 7–12.

1029 Bruand, E., Storey, C. & Fowler, M. (2014). Accessory mineral chemistry of high Ba-Sr
1030 granites from Northern Scotland: Constraints on petrogenesis and records of whole-rock
1031 Signature. *Journal of Petrology* **55**, 1619–1651.

1032 Bruand, E., Storey, C. & Fowler, M. (2016). An apatite for progress: Inclusions in zircon and
1033 titanite constrain petrogenesis and provenance. *Geology* **44**, 91–94.

1034 Burt, D. M. & Ferry, J. M. (1982). *Characterization of metamorphism through mineral*
1035 *equilibria*. Mineralogical Society of America.

1036 Caby, R. (1995). Plastic deformation of gabbros in a slow-spreading Mesozoic ridge:
1037 Example of the Montgenevre ophiolite, Western Alps. *Mantle and Lower crust exposed*

in oceanic ridges and in ophiolites. Springer, 123–145.

Castelli, D. & Rubatto, D. (2002). Stability of Al- and F-rich titanite in metacarbonate: Petrologic and isotopic constraints from a polymetamorphic eclogitic marble of the internal Sesia zone (Western Alps). *Contributions to Mineralogy and Petrology* **142**, 627–639.

Cave, B. J., Stepanov, A. S., Large, R. R., Halpin, J. A. & Thompson, J. (2015). Release of trace elements through the sub-greenschist facies breakdown of detrital rutile to metamorphic titanite in the Otago Schist, New Zealand. *Canadian Mineralogist* **53**, 379–400.

Chen, Y. X. & Zheng, Y. F. (2015). Extreme Nb/Ta fractionation in metamorphic titanite from ultrahigh-pressure metagranite. *Geochimica et Cosmochimica Acta*. Elsevier Ltd **150**, 53–73.

Cherniak, D. J. (2015). Nb and Ta diffusion in titanite. *Chemical Geology*. Elsevier B.V. **413**, 44–50.

Cisneros, M., Ashley, K. T. & Bodnar, R. J. (2020). Evaluation and application of the quartz-inclusions-in-epidote mineral barometer. *American Mineralogist* **105**, 1140–1151.

Clark, C., Taylor, R. J. M., Johnson, T. E., Harley, S. L., Fitzsimons, I. C. W. & Oliver, L. (2019). Testing the fidelity of thermometers at ultrahigh temperatures. *Journal of Metamorphic Geology* **37**, 917–934.

Clarke, G. L., Powell, R. & Fitzherbert, J. A. (2006). The lawsonite paradox: A comparison of field evidence and mineral equilibria modelling. *Journal of Metamorphic Geology* **24**, 715–725.

Corno, A., Groppo, C., Borghi, A., Mosca, P. & Gattiglio, M. (2023). To be or not to be

Alpine: New petrological constraints on the metamorphism of the Chenaillet Ophiolite (Western Alps). *Journal of Metamorphic Geology*.

Cruciani, G., Fancello, D., Franceschelli, M., Massonne, H. J., Langone, A. & Scodina, M. (2020). Geochemical and geochronological dataset of rutile from a Variscan metabasite in Sardinia, Italy. *Data in Brief*. Elsevier Inc. **31**.

Cruz-Uribe, A. M., Feineman, M. D., Zack, T. & Jacob, D. E. (2018). Assessing trace element (dis)equilibrium and the application of single element thermometers in metamorphic rocks. *Lithos*. Elsevier B.V. **314**–**315**, 1–15.

Deville, E., Fudral, S., Lagabrielle, Y., Marthaler, M. & Sartori, M. (1992). From oceanic closure to continental collision: A synthesis of the" Schistes lustrés" metamorphic complex of the Western Alps. *Geological Society of America Bulletin*. Geological Society of America **104**, 127–139.

El Korh, A., Schmidt, S. T., Ulianov, A. & Potel, S. (2009). Trace element partitioning in HP-LT metamorphic assemblages during subduction-related metamorphism, Ile de Groix, France: A detailed LA-ICPMS study. *Journal of Petrology* **50**, 1107–1148.

Enami, M., Nishiyama, T. & Mouri, T. (2007). Laser Raman microspectrometry of metamorphic quartz: A simple method for comparison of metamorphic pressures. *American Mineralogist* **92**, 1303–1315.

Engi, M. (2017). Petrochronology Based on REE-Minerals: Monazite, Allanite, Xenotime, Apatite. *Reviews in Mineralogy and Geochemistry* **83**, 365–418.

Escudero, A., Langenhorst, F. & Müller, W. F. (2012). Aluminum solubility in TiO2 rutile at high pressure and experimental evidence for a CaCl2-structured polymorph. *American Mineralogist* **97**, 1075–1082.

1084 Ewing, T. A., Rubatto, D. & Hermann, J. (2014). Hafnium isotopes and Zr/Hf of rutile and
1085 zircon from lower crustal metapelites (Ivrea-Verbano Zone, Italy): Implications for
1086 chemical differentiation of the crust. *Earth and Planetary Science Letters*. Elsevier B.V.
1087 **389**, 106–118.

1088 Force, E. R. (1991). *Geology of titanium-mineral deposits*. Geological Society of America.

1089 Fournier, M., Jolivet, L., Goffé, B. & Dubois, R. (1991). Alpine Corsica metamorphic core
1090 complex. *Tectonics*. Wiley Online Library **10**, 1173–1186.

1091 Frost, B. R., Chamberlain, K. R. & Schumacher, J. C. (2001). Sphene (titanite): Phase
1092 relations and role as a geochronometer. *Chemical Geology* **172**, 131–148.

1093 Gao, C., Liu, Y., Zong, K., Hu, Z. & Gao, S. (2010). Microgeochemistry of rutile and zircon
1094 in eclogites from the CCSD main hole: Implications for the fluid activity and thermo-
1095 history of the UHP metamorphism. *Lithos*. Elsevier B.V. **115**, 51–64.

1096 Gao, S. *et al.* (2004). Recycling lower continental crust in the North China craton. *Nature*
1097 **432**, 892–897.

1098 Garber, J. M., Hacker, B. R., Kylander-Clark, A. R. C., Stearns, M. & Seward, G. (2017).
1099 Controls on trace element uptake in metamorphic titanite: Implications for
1100 petrochronology. *Journal of Petrology* **58**, 1031–1057.

1101 Goldsmith, R. & Force, E. R. (1978). Distribution of rutile in metamorphic rocks and
1102 implications for placer deposits. *Mineralium Deposita* **13**, 329–343.

1103 Gonzalez, J. P. (2019). Applications of Elastic Modeling , Thermobarometry , and Thermal
1104 History Modeling to (Ultra) high-Pressure Metamorphic Rocks. .

1105 Gonzalez, J. P., Mazzucchelli, M. L., Angel, R. J. & Alvaro, M. (2021). Elastic Geobarometry
1106 for Anisotropic Inclusions in Anisotropic Host Minerals: Quartz-in-Zircon. *Journal of*

Geophysical Research: Solid Earth **126**.

Green, E. C. R., White, R. W., Diener, J. F. A., Powell, R., Holland, T. J. B. & Palin, R. M. (2016). Activity–composition relations for the calculation of partial melting equilibria in metabasic rocks. *Journal of Metamorphic Geology* **34**, 845–869.

Groppo, C. & Castelli, D. (2010). Prograde P-T evolution of a lawsonite eclogite from the Monviso meta-ophiolite (Western Alps): Dehydration and redox reactions during subduction of oceanic FeTi-oxide gabbro. *Journal of Petrology* **51**, 2489–2514.

Guo, R., Hu, X., Garzanti, E., Lai, W., Yan, B. & Mark, C. (2020). How faithfully do the geochronological and geochemical signatures of detrital zircon, titanite, rutile and monazite record magmatic and metamorphic events? A case study from the Himalaya and Tibet. *Earth-Science Reviews*. Elsevier **201**, 103082.

Guo, S., Tang, P., Su, B., Chen, Y., Ye, K., Zhang, L., Gao, Y., Liu, J. & Yang, Y. (2017). Unusual replacement of Fe-Ti oxides by rutile during retrogression in amphibolite-hosted veins (Dabie UHP terrane): A mineralogical record of fluid-induced oxidation processes in exhumed UHP slabs. *American Mineralogist* **102**, 2268–2283.

Hart, E., Storey, C., Bruand, E., Schertl, H. P. & Alexander, B. D. (2016). Mineral inclusions in rutile: A novel recorder of HP-UHP metamorphism. *Earth and Planetary Science Letters* **446**, 137–148.

Hart, E., Storey, C., Harley, S. L. & Fowler, M. (2018). A window into the lower crust: Trace element systematics and the occurrence of inclusions/intergrowths in granulite-facies rutile. *Gondwana Research*. Elsevier B.V. **59**, 76–86.

Holder, R. M. & Hacker, B. R. (2019). Fluid-driven resetting of titanite following ultrahigh-temperature metamorphism in southern Madagascar. *Chemical Geology*. Elsevier **504**,

38–52.

Holycross, M. & Cottrell, E. (2020). Partitioning of V and 19 other trace elements between rutile and silicate melt as a function of oxygen fugacity and melt composition: Implications for subduction zones. *American Mineralogist* **105**, 244–254.

Holycross, M. & Cottrell, E. (2022). Experimental quantification of vanadium partitioning between eclogitic minerals (garnet , clinopyroxene , rutile) and silicate melt as a function of temperature and oxygen fugacity. *Contributions to Mineralogy and Petrology*. Springer Berlin Heidelberg **177**, 1–23.

Hoschek, G. (1969). The stability of staurolite and chloritoid and their significance in metamorphism of pelitic rocks. *Contributions to Mineralogy and Petrology*. Springer **22**, 208–232.

Kelemen, P. *et al.* (2004). ODP Leg 209 drills into mantle peridotite along the Mid-Atlantic Ridge from 14 N to 16 N. .

Kendrick, J. & Indares, A. (2018). The Ti record of quartz in anatectic aluminous granulites. *Journal of Petrology* **59**, 1493–1516.

Kooijman, E., Smit, M. A., Mezger, K. & Berndt, J. (2012). Trace element systematics in granulite facies rutile: Implications for Zr geothermometry and provenance studies. *Journal of Metamorphic Geology* **30**, 397–412.

Lahondère, D. & Guerrot, C. (1997). Sm-Nd dating of Alpine eclogitic metamorphism in Corsica: evidence for Late Cretaceous subduction beneath The Corsican Sardinian Block. *Géologie de la France* **3**, 3–11.

Liou, J. G., Zhang, R., Ernst, W. G., Liu, J. & McLimans, R. (1998). Mineral parageneses in the Piampaludo eclogitic body, Gruppo di Voltri, western Ligurian Alps. *Schweizerische*

Mineralogische und Petrographische Mitteilungen **78**, 317–335.

Manatschal, G., Sauter, D., Karpoff, A. M., Masini, E., Mohn, G. & Lagabrielle, Y. (2011). The Chenaillet Ophiolite in the French/Italian Alps: An ancient analogue for an Oceanic Core Complex? *Lithos*. Elsevier B.V. **124**, 169–184.

Marsh, J. H. & Smye, A. J. (2017). U-Pb systematics and trace element characteristics in titanite from a high-pressure mafic granulite. *Chemical Geology* **466**, 403–416.

Marthaler, M. & Stampfli, G. M. (1989). Les Schistes lustrés à ophiolites de la nappe du Tsaté: un ancien prisme d'accrétion issu de la marge active apulienne? *Schweizerische Mineralogische und Petrographische Mitteilungen* **69**, 211–216.

Martin, L. A. J., Hermann, J., Gauthiez-Putallaz, L., Whitney, D. L., Vitale Brovarone, A., Fornash, K. F. & Evans, N. J. (2014). Lawsonite geochemistry and stability - implication for trace element and water cycles in subduction zones. *Journal of Metamorphic Geology* **32**, 455–478.

McDonough, W. F. & Sun, S. s. (1995). The composition of the Earth. *Chemical Geology* **120**, 223–253.

Meinhold, G., Anders, B., Kostopoulos, D. & Reischmann, T. (2008). Rutile chemistry and thermometry as provenance indicator: An example from Chios Island, Greece. *Sedimentary Geology* **203**, 98–111.

Miller, C., Zanetti, A., Thöni, M. & Konzett, J. (2007). Eclogitisation of gabbroic rocks: Redistribution of trace elements and Zr in rutile thermometry in an Eo-Alpine subduction zone (Eastern Alps). *Chemical Geology* **239**, 96–123.

Nehring, F., Foley, S. F. & Hölttä, P. (2010). Trace element partitioning in the granulite facies. *Contributions to Mineralogy and Petrology* **159**, 493–519.

1176 Ng, Y. N., Shi, G. H. & Santosh, M. (2016). Titanite-bearing omphacitite from the Jade Tract,
1177 Myanmar: Interpretation from mineral and trace element compositions. *Journal of Asian*
1178 *Earth Sciences*. Elsevier Ltd **117**, 1–12.

1179 Palin, R. M., Santosh, M., Cao, W., Li, S., Hernández-uribe, D. & Parsons, A. (2020). Secular
1180 metamorphic change and the onset of plate tectonics. *Earth-Science Reviews*. Elsevier
1181 **207**, 103172.

1182 Pereira, I., Storey, C. D., Strachan, R. A., Bento dos Santos, T. & Darling, J. R. (2020).
1183 Detrital rutile ages can deduce the tectonic setting of sedimentary basins. *Earth and*
1184 *Planetary Science Letters*. Elsevier B.V. **537**, 116193.

1185 Pereira, I., Storey, C., Darling, J., Lana, C. & Alkmim, A. R. (2019). Two billion years of
1186 evolution enclosed in hydrothermal rutile: Recycling of the São Francisco Craton Crust
1187 and constraints on gold remobilisation processes. *Gondwana Research*. Elsevier B.V. **68**,
1188 69–92.

1189 Rampone, E., Hofmann, A. W. & Raczek, I. (2009). Isotopic equilibrium between mantle
1190 peridotite and melt: Evidence from the Corsica ophiolite. *Earth and Planetary Science*
1191 *Letters*. Elsevier B.V. **288**, 601–610.

1192 Rizzo, G., Canora, F., Dichicco, M. C., Laurita, S. & Sansone, M. T. C. (2019). P-T estimates
1193 from amphibole and plagioclase pairs in metadolerite dykes of the Frido unit (southern
1194 Apennines-Italy) during the ocean-floor metamorphism. *Journal of Mediterranean Earth*
1195 *Sciences* **11**, 31–45.

1196 Robinson, P. T., Dick, H. J. B. & Von Herzen, R. (1991). 27. Metamorphism And Alteration
1197 In Oceanic Layer 3: Hole 735B1. *Proceedings of the Ocean Drilling Program*. National
1198 Science Foundation Washington, DC, 541–552.

1199 Rubatto, D. (2002). Zircon trace element geochemistry: partitioning with garnet and the link
1200 between U–Pb ages and metamorphism. *Chemical geology*. Elsevier **184**, 123–138.

1201 Rubatto, D. & Hermann, J. (2001). Exhumation as fast as subduction? *Geology*. Geological
1202 Society of America **29**, 3–6.

1203 Rubatto, D., Regis, D., Hermann, J., Boston, K., Engi, M., Beltrando, M. & Mcalpine, S. R.
1204 B. (2011). Yo-yo subduction recorded by accessory minerals in the Italian Western Alps
1205 Daniela. *Nature Geoscience*. Nature Publishing Group **4**, 1–5.

1206 Ryerson, F. J. & Watson, E. B. (1987). Rutile saturation in magmas: implications for TiNbTa
1207 depletion in island-arc basalts. *Earth and Planetary Science Letters* **86**, 225–239.

1208 Saccani, E., Principi, G., Garfagnoli, F. & Menna, F. (2008). Corsica ophiolites:
1209 Geochemistry and petrogenesis of basaltic and metabasaltic rocks. *Ofioliti* **33**, 187–207.

1210 Sassi, R., Harte, B., Carswell, D. A. & Yujing, H. (2000). Trace element distribution in
1211 Central Dabie eclogites. *Contributions to Mineralogy and Petrology* **139**, 298–315.

1212 Schwartz, S., Guillot, S., Reynard, B., Lafay, R., Debret, B., Nicollet, C., Lanari, P. &
1213 Auzende, A. L. (2013). Pressure–temperature estimates of the lizardite/antigorite
1214 transition in high pressure serpentinites. *Lithos*. Elsevier **178**, 197–210.

1215 Scibiorski, E. A. & Cawood, P. A. (2022). Titanite as a petrogenetic indicator. *Terra Nova* **34**,
1216 177–183.

1217 Scibiorski, E., Kirkland, C. L., Kemp, A. I. S., Tohver, E. & Evans, N. J. (2019). Trace
1218 elements in titanite: A potential tool to constrain polygenetic growth processes and
1219 timing. *Chemical Geology* **509**, 1–19.

1220 Spandler, C., Hermann, J., Arculus, R. & Mavrogenes, J. (2003). Redistribution of trace
1221 elements during prograde metamorphism from lawsonite blueschist to eclogite facies;

implications for deep subduction-zone processes. *Contributions to Mineralogy and Petrology* **146**, 205–222.

Spear, F. S. (1981). An experimental study of hornblende stability and compositional variability in amphibolite. *American Journal of Science*, 697–734.

Spear, F. S. (1993). *Metamorphic phase equilibria and pressure-temperature-time paths*. *Mineralogical Society of America Monograph*. Mineralogical Society of America.

Staudigel, H. & Hart, S. R. (1983). Alteration of basaltic glass: Mechanisms and significance for the oceanic crust-seawater budget. *Geochimica et Cosmochimica Acta*. Elsevier **47**, 337–350.

Toplis, M. J. & Carroll, M. R. (1995). An experimental study of the influence of oxygen fugacity on fe-ti oxide stability, phase relations, and mineral-melt equilibria in ferro-basaltic systems. *Journal of Petrology* **36**, 1137–1170.

Tribuzio, R., Manatschal, G., Renna, M. R., Ottolini, L. & Zanetti, A. (2019). Tectono-magmatic Interplay and Related Metasomatism in Gabbros of the Chenaillet Ophiolite (Western Alps). *Journal of Petrology*. Oxford University Press **60**, 2483–2508.

Tribuzio, R., Tiepolo, M. & Thirlwall, M. F. (2000). Origin of titanian pargasite in gabbroic rocks from the Northern Apennine ophiolites (Italy): Insights into the late-magmatic evolution of a MOR-type intrusive sequence. *Earth and Planetary Science Letters* **176**, 281–293.

Tropper, P., Manning, C. E. & Essene, E. J. (2002). The Substitution of Al and F in Titanite at High Pressure and Temperature : Experimental Constraints on Phase Relations and Solid Solution Properties. *Journal of Petrology* **43**, 1787–1814.

Vitale Brovarone, A. & Agard, P. (2013). True metamorphic isograds or tectonically sliced

metamorphic sequence? New high-spatial resolution petrological data for the New Caledonia case study. *Contributions to Mineralogy and Petrology* **166**, 451–469.

Vitale Brovarone, A., Groppo, C., Hetényi, G., Compagnoni, R. & Malavieille, J. (2011). Coexistence of lawsonite-bearing eclogite and blueschist: Phase equilibria modelling of Alpine Corsica metabasalts and petrological evolution of subducting slabs. *Journal of Metamorphic Geology* **29**, 583–600.

Vitale Brovarone, A. & Herwartz, D. (2013). Timing of HP metamorphism in the Schistes Lustrés of Alpine Corsica: New Lu-Hf garnet and lawsonite ages. *Lithos*. Elsevier B.V. **172**–**173**, 175–191.

Whitaker, M. L., Nekvasil, H., Lindsley, D. H. & Difrancesco, N. J. (2007). The role of pressure in producing compositional diversity in intraplate basaltic magmas. *Journal of Petrology* **48**, 365–393.

White, R. W., Powell, R., Holland, T. J. B., Johnson, T. E. & Green, E. C. R. (2014). New mineral activity–composition relations for thermodynamic calculations in metapelitic systems. *Journal of Metamorphic Geology*. Wiley Online Library **32**, 261–286.

Whitney, D. L. & Davis, P. B. (2006). Why is lawsonite eclogite so rare? Metamorphism and preservation of lawsonite eclogite, Sivrihisar, Turkey. *Geology* **34**, 473–476.

Xiao, X., Zhou, T., White, N. C., Zhang, L., Fan, Y. & Chen, X. (2020). Multiple generations of titanites and their geochemical characteristics record the magmatic-hydrothermal processes and timing of the Dongguashan porphyry-skarn Cu-Au system, Tongling district, Eastern China. *Mineralium Deposita*. Mineralium Deposita.

Xiao, Y., Niu, Y., Li, H., Wang, H., Liu, X. & Davidson, J. (2014). Trace element budgets and (re-)distribution during subduction-zone ultrahigh pressure metamorphism: Evidence

from Western Tianshan, China. *Chemical Geology*. Elsevier B.V. **365**, 54–68.

Yakymchuk, C. (2017). Behaviour of apatite during partial melting of metapelites and consequences for prograde suprasolidus monazite growth. *Lithos*. Elsevier **274**, 412–426.

Zack, T., Kronz, A., Foley, S. F. & Rivers, T. (2002). Trace element abundances in rutiles from eclogites and associated garnet mica schists. *Chemical Geology* **184**, 97–122.

Zeh, A., Cabral, A. R., Koglin, N. & Decker, M. (2018). Rutile alteration and authigenic growth in metasandstones of the Moeda Formation, Minas Gerais, Brazil – A result of Transamazonian fluid–rock interaction. *Chemical Geology*. Elsevier B.V **483**, 397–409.

Zhou, G., Fisher, C. M., Luo, Y., Pearson, D. G., Li, L., He, Y. & Wu, Y. (2020). A clearer view of crustal evolution: U-Pb, Sm-Nd, and Lu-Hf isotope systematics in five detrital minerals unravel the tectonothermal history of northern China. *GSA Bulletin* 1–15.

1289 *Table 1. Sampling details.*

Grade	**LP-HT (IODP)**					**LP-HT (W. ALPS)**			**HP-LT**			**HP-MT**					
Samples	1316	1318	1320	1319	5450	CH1	CH3	CHDI	QE01	QE06	TR10	C16	Cv16	C147	PG	LS	VE29
Locality	LEG 209			305	118	Chenaillet Massif			Queyras			Corsica			Passo Gallarino	Lago Superiore	Verne Monviso
T (°C)	740 - 840				-	700-900			330 - 400		380 - 470	500 - 550			450; 525	550 - 600	500-550
P (kbar)	< 2					< 2			11 - 15		12 - 18	21 - 24			12; 25-29	19; 25 - 27	21-27
Ref.	This study					This study; G			E		A	F			C; B	C; B	D

A. *Debret* et al., *2016*; B – *Angiboust* et al., *2012*; C. *Schwartz* et al., *2000*; D. *Groppo and Castelli, 2010*; E. *Agard* et al., *2001*; F. Vitale-Brovarone et al. 2011; G. *Mevél* et al., *1978*.

1290

1291

Table 2. Paragenetic chart of the studied samples, organised by metamorphic grade, from LP-H/MT to HP-LT and HP-MT. The peak assemblage represents the highest metamorphic grade each rock attained.

	LP – H/MT								HP – L/MT								
Samples/ Minerals	13 16	13 18	13 19	13 20	54 50	CH1	CH3	CH DI	QE-01	QE-06	TR 10	C 16	C v 16	C 147	PG	LS	VE 29
Augite	m	m	m		m	m				m							
Plagioclase	m	m	m	m	m												
Hornblende[a]	x	x		x	x	x	x										
Heden-Diopside			x														
Garnet													x	x		x	x
Omphacite													x	x	x	x	x
Hornblende[b]	x	x	x	x	x	x	x		x	x							
Actinolite						ret	ret	x	x								
Glaucophane[c]									x	x	x	x	x	x	x		
Epidote					x				x	x	x	x		x	x	x	x
Lawsonite									x	x	x		x	x			
Albite		ret	ret	ret		ret	ret	x	ret	ret	ret	ret					
Quartz	x									x		x		x	x	x	x
white mica										x	x				x	x	x
Ilmenite		m/x	m/x	m/x	m/x	x	x	x			x				x	x	x
Rutile	x i		x i	x i	x i	x i	x i	x i	i	i	i				x	x	x
Titanite	x	x	x ov	x ov	x	x	x	x	x	x	x	x	x	x	ret		
Chlorite	ret				ret	ret					x		ret				
Carbonate	ret		ret		ret					ret	ret						

Note that some minerals indicated on the list are one possible end-member. a. another equivalent brown amphibole; b. another equivalent green amphibole; c. another equivalent blue Na, Na-Ca amphibole. In the table, m – magmatic, x – metamorphic and i – inclusion, ov – overgrowth, ret – late retrograde phase

1296 *Table 3. Titanite trace element compositions summary.*

	∑REE	∑LREE	La/SmN	Eu/Eu*	Th/U
Amphibolite	*10 - 3358*	*2.6 - 2400*	*0.02 - 1.2*	*0.2 - 29*	*0.01 - 0.48*
Granulite*	*13 - 2000*	*11 - 1678*	*5 - 93*	*4.7 - 314*	*0.08 - 1.06*
Blueschist	*32 - 370*	*3.8 - 59*	*0.02 - 0.7*	*0.9 - 3.2*	*0.04 - 0.2*
Eclogite	*168 - 465*	*20 - 208*	*0.02 - 0.3*	*0.84 - 1.8*	*0.004 – 2.3*

REE sums are in ppm. Data was normalized to Sun and McDonough (1995) Chondrite values. Amphibolite corresponds to a combination of Ch3 and IODP1319, granulite to IODP1320, blueschist to a combination of QE1, QE6, TR10, and eclogite to C147, C16v and C16 data. *titanite in the granulite sample is most probably formed at lower temperatures, but the sample rock forming minerals did not retrogress to those conditions.

1297
1298
1299
1300
1301
1302
1303
1304
1305
1306
1307
1308
1309
1310
1311
1312
1313
1314
1315
1316
1317
1318

1319 Figure captions
1320

1321 *Figure 1 Experimental vs pseudosection modelling diagrams for a MORB composition and focusing on Ti-*
1322 *phases.* ***A.*** *P-T diagram highlighting the fields of known stability of rutile, titanite and ilmenite for MORB*
1323 *compositions (Liou et al., 1998). In white a field of no experimental data available for mafic compositions. Grey*
1324 *lines delimit different metamorphic facies. Two dotted lines separate the fields of low (< 440 ºC/GPa) from*
1325 *moderate and higher geothermal gradient (> 770 ºC/GPa) (Palin et al., 2020). Boxes correspond to*
1326 *approximate peak P-T conditions from samples collected for this study, highlighting cooling of amphibole-*
1327 *bearing gabbros from the oceanic crust, and burial history of blueschist and eclogite rocks from the Alpine*
1328 *chain.* ***B****. MORB phase diagram modelling from Green et al. (2016) showing titanite-out reaction (in green),*
1329 *solid blue line the same as in a) and a dotted white line at 600 ºC, below which there are no data constraints on*
1330 *Ti-phase stability for mafic compositions (taken from inset a).*

1331 *Figure 2. Sampling locations in the Western Alps and Corsica (A, B) and from IODP drilling sites (C). Western*
1332 *Alps maps were modified after Angiboust et al., (2012), Debret et al. (2016), Locatelli et al., (2019), and Vitale-*
1333 *Brovarone et al., (2011), and IODP drilling site information and map were modified from data and maps*
1334 *available at iodp.org.*

1335 *Figure 3. Microphotographs of samples from IODP using PPL (A, C, G, H), reflected light (D- E) and BSE*
1336 *imaging (B, F). A-B, occurrence of sub-spherical rutile grains rimmed by titanite enclosed by altered*
1337 *plagioclase and brown to green amphibole; C, occurrence of large ilmenite grains rimmed by titanite; E-F*
1338 *ilmenite-rutile-titanite grains, with titanite replacing former ilmenite usually found at the cores; F is a zoom in*
1339 *of E, illustrating the occurrence of rutile rimmed by ilmenite and only then by titanite; G-H, occurrence of*
1340 *idioblastic titanite associated with altered plagioclase and brownish-green amphibole.*

1341 *Figure 4. Microphotographs of samples from the Chenaillet Massif using PPL (A-D, G), reflected light (E, F)*
1342 *and BSE imaging (H). A and B, general textural and mineralogical relationships; C, of the late-stage titanite*
1343 *and actinolite shear zone in Ch1; D-F. detail of ilmenite-rutile-titanite occurrences in ChDi; G-H ilmenite-*
1344 *titanite growth in the shear zone, and strong BSE zoning in these titanite grains.*

1345 *Figure 5. Microphotographs of blueschist samples from the W. Alps in the Queyras using PPL (A, B, C),*
1346 *reflected light (D) and BSE imaging (E, F). A- plagioclase domains with lawsonite, albite and epidote, and relic*
1347 *magmatic clinopyroxene replaced by glaucophane and epidote and titanite. B- overgrowth of actinolite on*

glaucophane in plagioclase sites, with titanite. C-F, titanite grains with very fine-grained lamellae rutile inclusions in all the different investigated samples.

Figure 6. Microphotographs of eclogite samples from the W. Alps in the Passo Gallarino-Monviso-Lago Superiore (A-D) and Corsica (E-H) using PPL (B, C, E-G), reflected light (A) and BSE imaging (D). A – in Passo Gallarino a thin rim of titanite is found around rutile; B- omphacite, garnet, and phengite associated to rutile; C – Foliated eclogite with omphacite, garnet, and rutile ribbons; D – a detail of a rutile ribbon from C with ilmenite/Fe-Ti oxide exsolution; E- blueschist eclogite, with albite, glaucophane crossed-cut by a vein showing omphacite, garnet, lawsonite and titanite; and G-H- eclogitic metabasalt with garnet, omphacite, lawsonite, glaucophane and titanite.

Figure 7. P-T diagram illustrating the conditions of either rutile or titanite stability found in the samples studied here. P-T constraints are from references found in table 1.

Figure 8. X_{Al} *vs* F_{apfu} *in titanite binary diagram. Different symbols and colours represent average titanite values from different samples. Green symbols are data from this study. Diamonds are for titanite from IODP samples, squares for the obducted Chenaillet metagabbro, circles for blueschist and triangles for eclogite titanite grains from this study. All other coloured symbols correspond to titanite data from other metamorphic grades and bulk-rock compositions that are plotted for comparison. Literature data from Franz and Spear, 1985, Markl and Piazolo, 1999, Ye et al., 2002, Castelli and Rubatto, 2002, Garber et al., 2017.*

Figure 9. Trace element diagrams for titanite, A) Nb/Ta vs Zr/Hf. Star refers to Chondrite compositions (Sun and McDonough, 1989); B) Sn vs V binary diagram. Diamonds correspond to IODP, squares to the Chenaillet Massif amphibolite metagabbro, circles to blueschist and triangles to eclogite rock titanite.

Figure 10. REE and Th/U values of titanite from HT and HP conditions.

Figure 71. Discrimination diagrams for rutile. A) The Cr-Nb discrimination modified from Meinhold et al. (2008). B) The Zr/Hf vs Nb/Ta modified from Pereira et al. (2019); C) based on PCA, the three main vectors V, Cr, Sc and Nb used in a ternary diagram; D) Binary diagram of the sum of HFSE ratios vs Nb/V. HT IODP are presented with two colours, the brighter red corresponding to sample 1320 and darker red to 1319 and 1316. Some labelled datapoints correspond to LA-ICP-MS acquired data used in Figure 11.

Figure 82. Rutile occurrence in amphibole-bearing gabbros on the oceanic crust (example from IODP1320); a) Reflected light microphotograph in grayscale of an ilmenite grain being replaced by titanite and rutile. Rutile

*occurs as exsolution lamellae and coarse grains; b) elemental concentrations of Zr and Cr in rutile from different textural domains labelled in part a). The symbol * correspond to a laser spot measurement.*

Figure 93. Binary trace element diagrams for ilmenite grains from samples IODP 1320 and 5450.

Figure 10. Composition in Ti/Ca and Ca/Al of several metagabbros, blueschist and eclogite rocks from different settings (IODP, Syros, Western Alps, Corsica) grouped by titanite, rutile or titanite-rutile stable (symbols). Range and average of unaltered MORB composition is given by the red circle and the red star respectively (Klein, 2004). Altered vectors correspond to altered MORB compositions from Zhang and Smith-Duque (2014). Corsica data are from Vitale-Brovarone et al. (2011) and Syros samples from Marschall (2005). Data used here can be found in the Supplementary Data: Electronic Appendix 1.

Figure 11. Trace element diagrams for titanite modified from Scibiorski et al. (2019). A. ∑HREE vs Y; B. Y vs Dy/Yb; In grey, labels adapted from Scibiorski et al. (2019) and in pink based on data from this study. Pink-coloured circles correspond to titanite grains in a garnet-bearing assemblage.

Figure 12. Ternary diagrams for titanite compositions from multiple geodynamic environments. Compiled literature data are from a. Bruand et al., 2014, b. Garber et al., 2017, c. Holder and Hacker, 2019, d. Marsh and Smye, 2017, e. selection of Scibiorski et al., 2019, f. Spandler et al., 2003, g. Ng et al. 2016, h. El Korh et al., 2009.

*Figure 13. Rutile discrimination diagrams for metamafic, gabbro in composition, rocks .a) is a V+Cr-Sc-Nb ternary and b) a V/Nb vs sum of HFSE ratios. Grey bar is highlighting some overlap between HP and LP signatures and arrow indicate the field towards HP rutile. a. relic in bs correspond to HT-LP rutile grains found as inclusions in blueschist titanite. Published data are from metamafic rocks b. and c. from blueschist and eclogite from Syros (*Hart *et al.*, 2016*), talc and lawsonite eclogite from Monviso* (Angiboust *et al.*, 2014) *and d. LP granulite* (*Cruciani et al., 2020*).

Figure 14. Ti-mineral phases in metagabbros and metabasalts associated to divergent and convergent settings and some of their main trace element systematics.

Fig. 1.

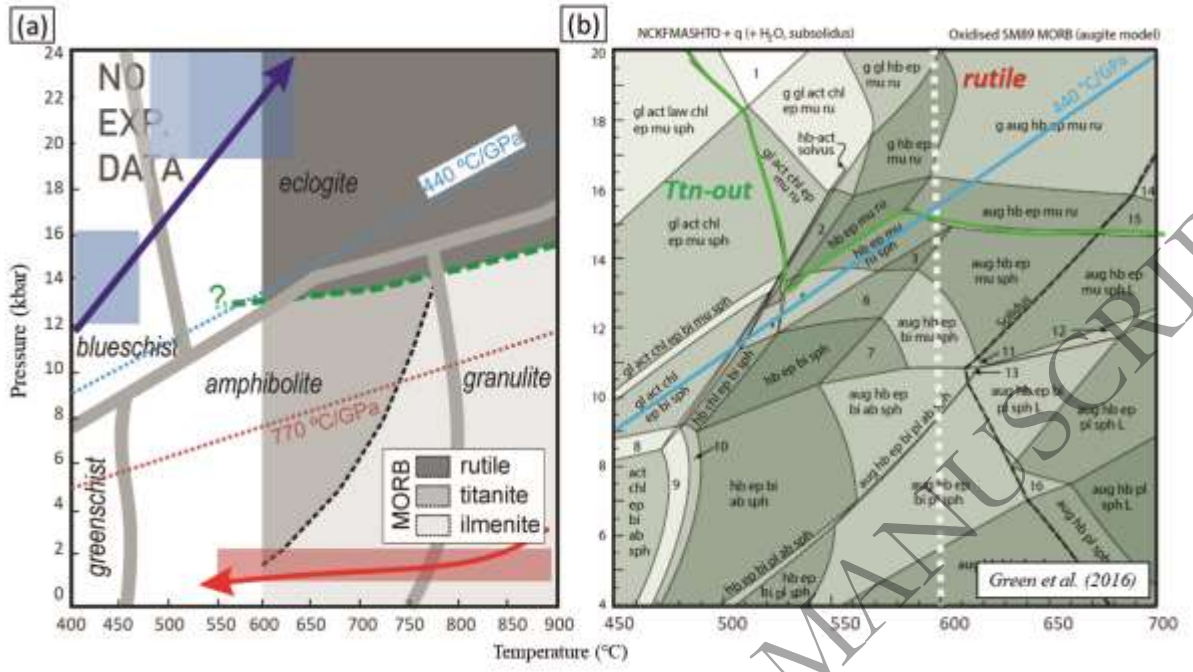

Fig. 2.

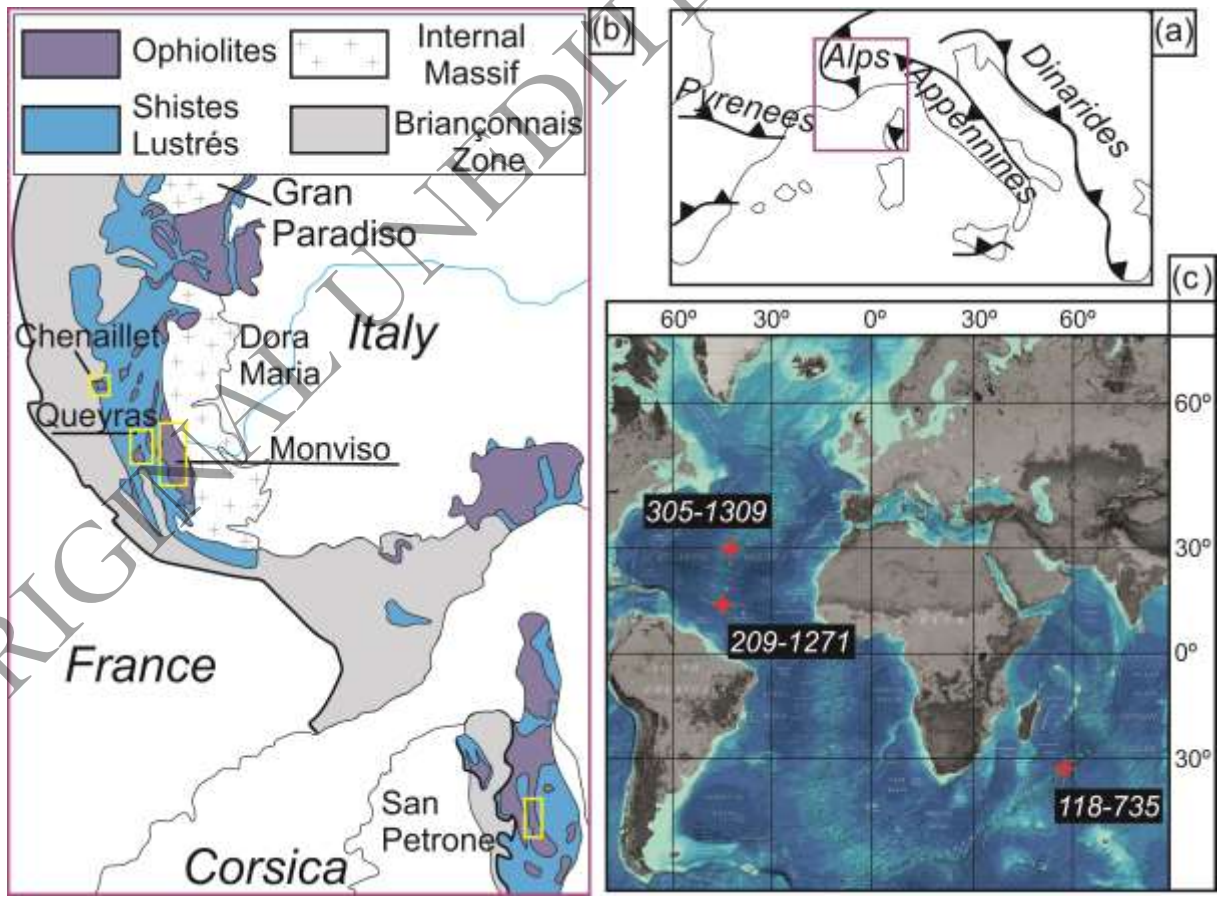

1409 **Fig. 3.**

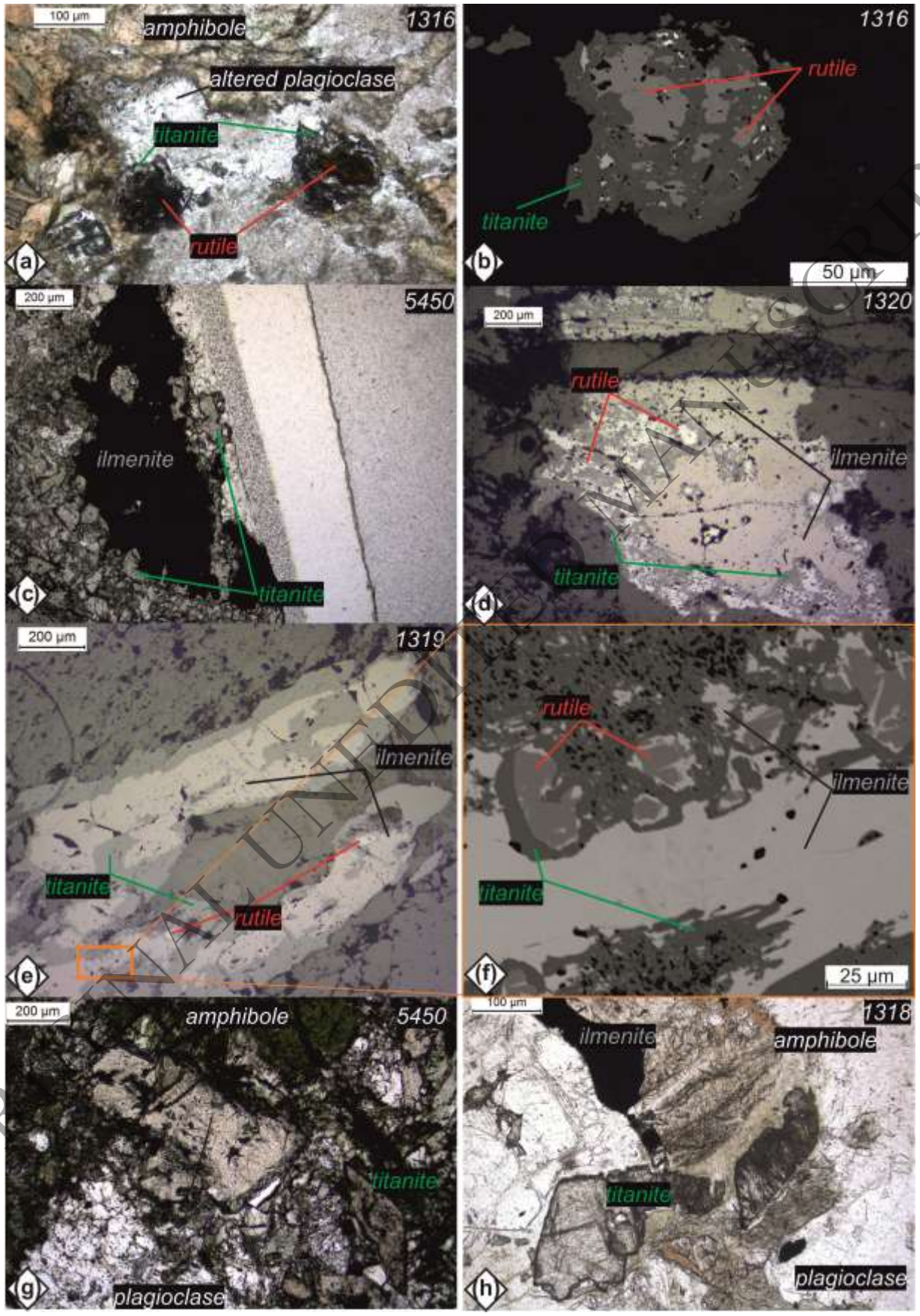

1410

1411

1412 **Fig. 4.**

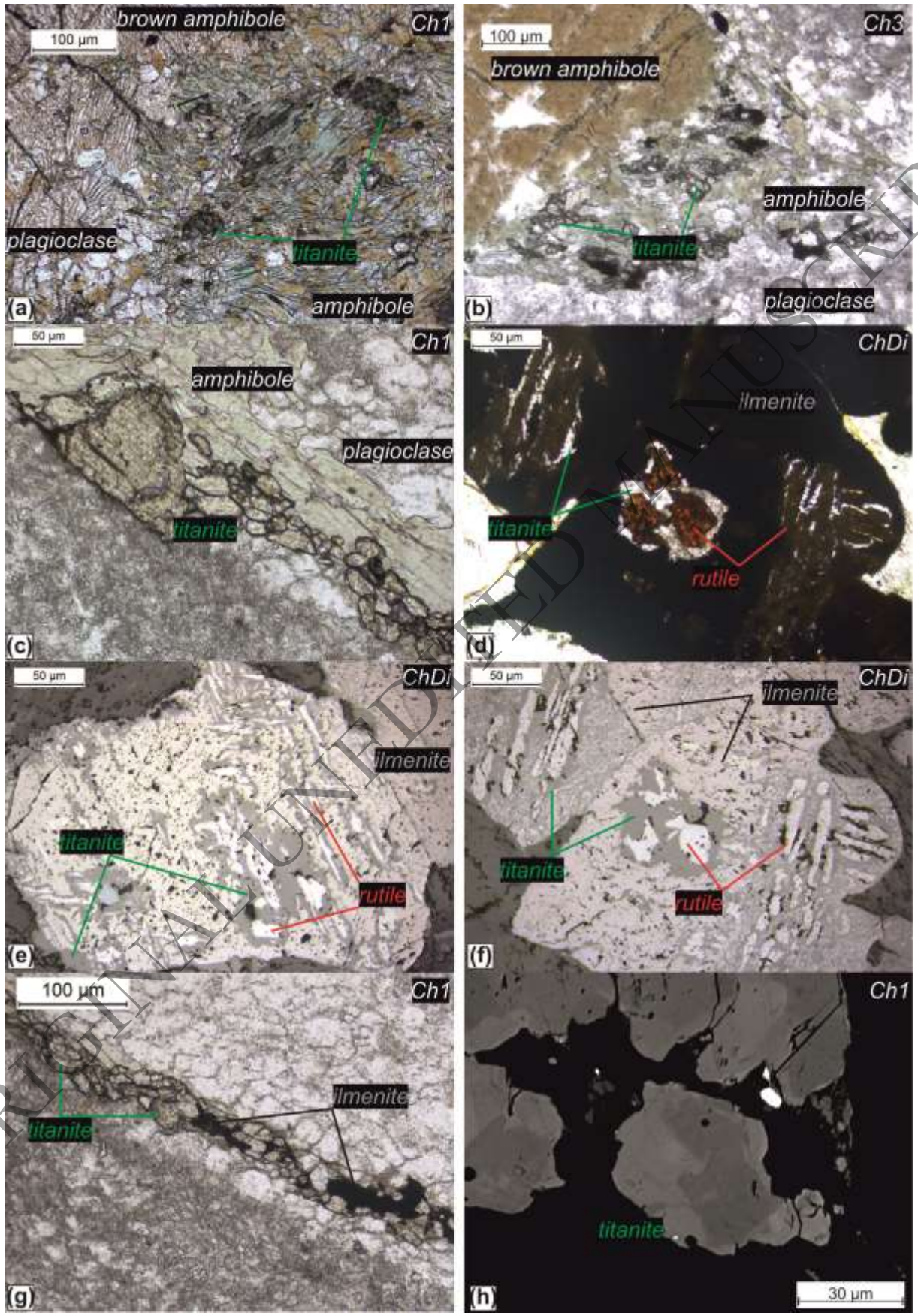

1413

Fig. 5.

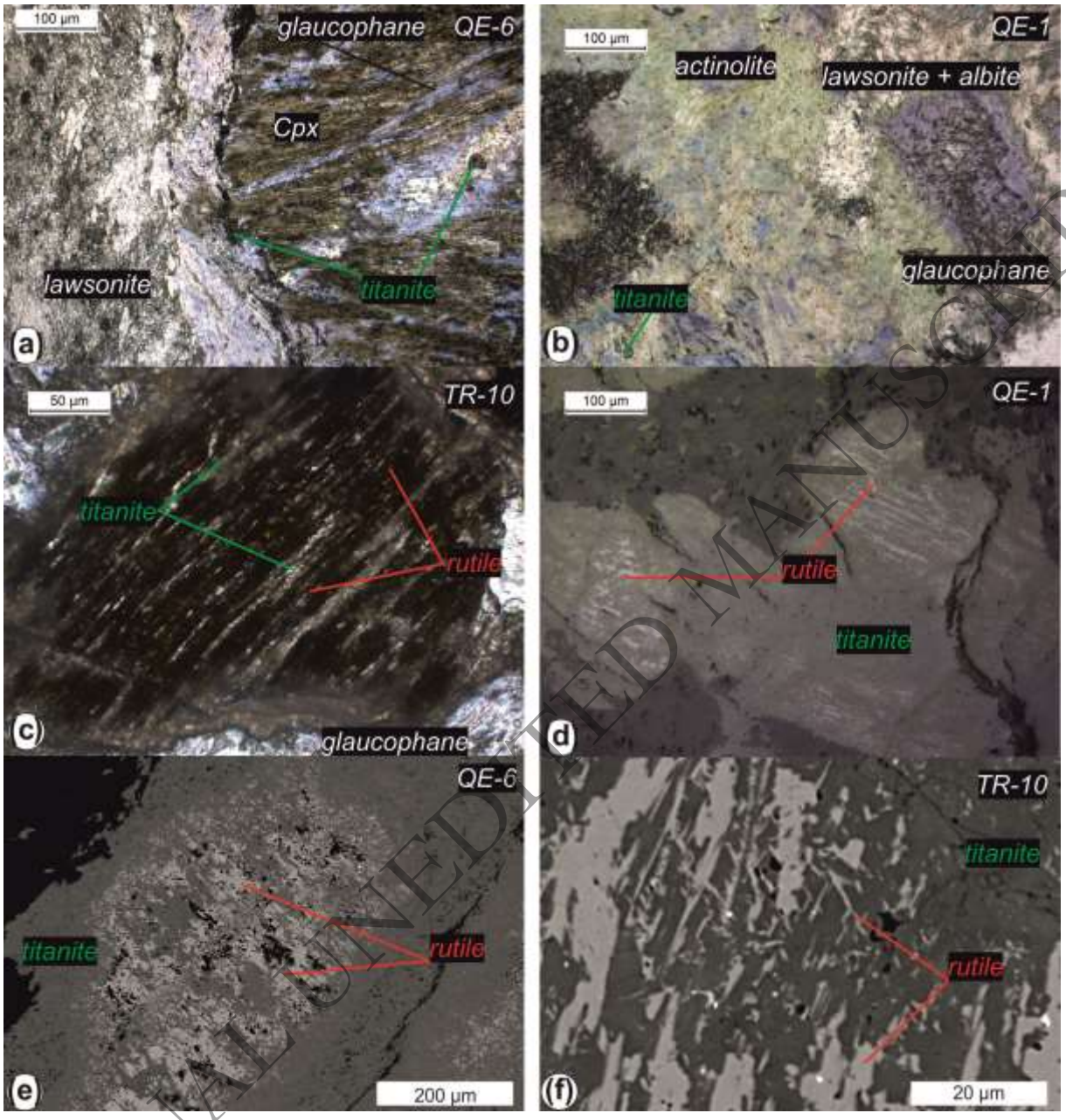

1424 **Fig. 6.**

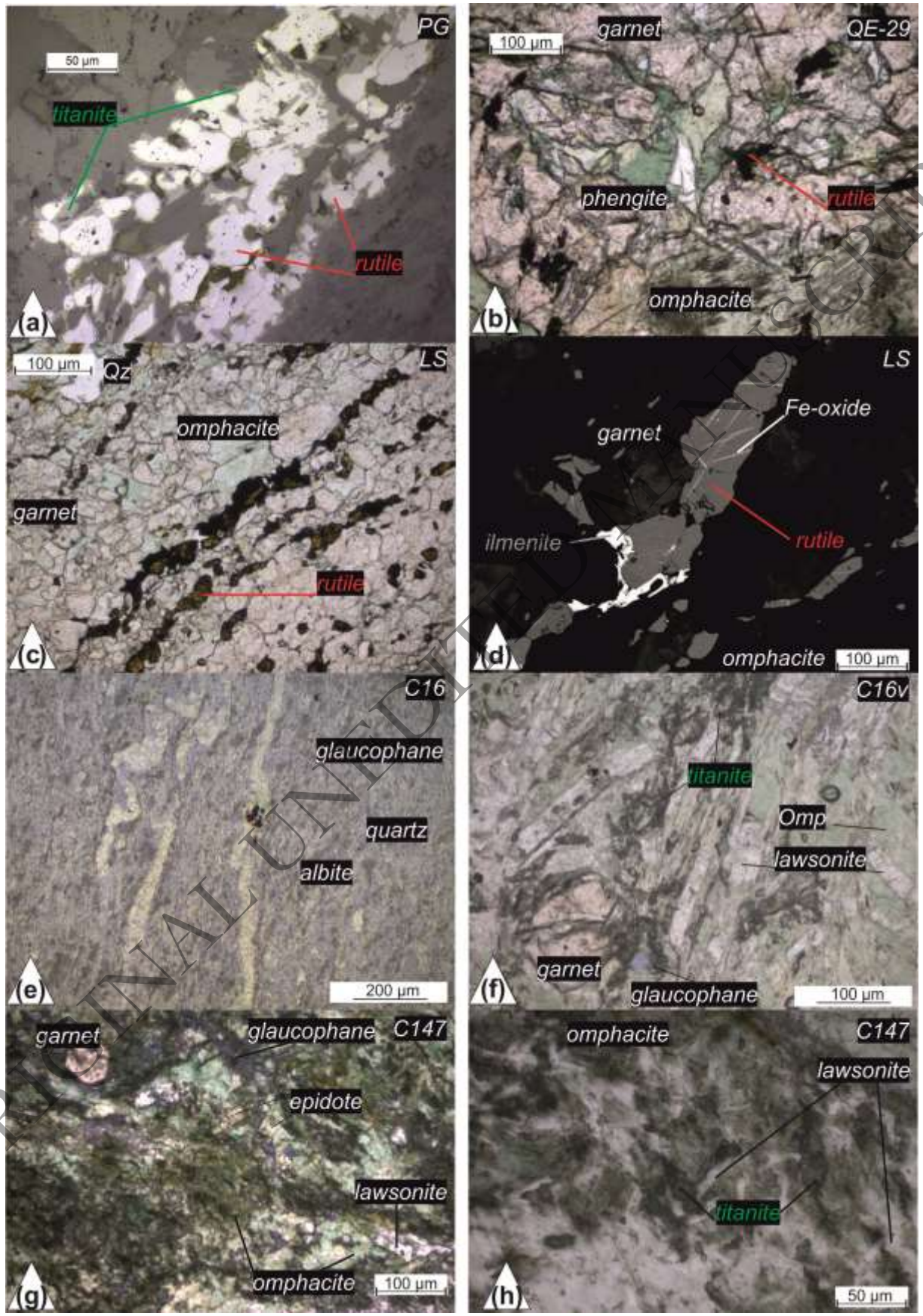

1425

1426

Fig. 7.

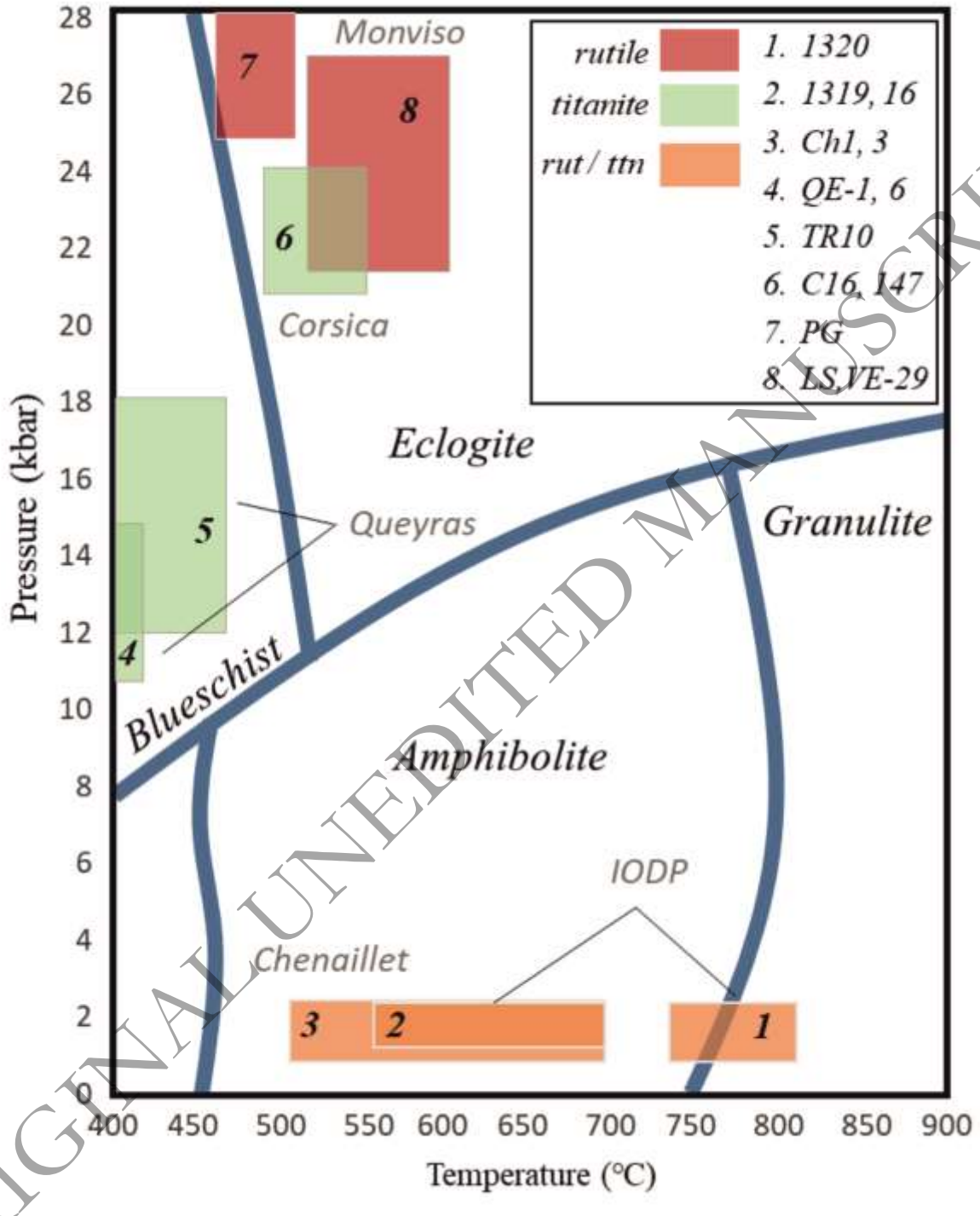

1434 **Fig. 8.**

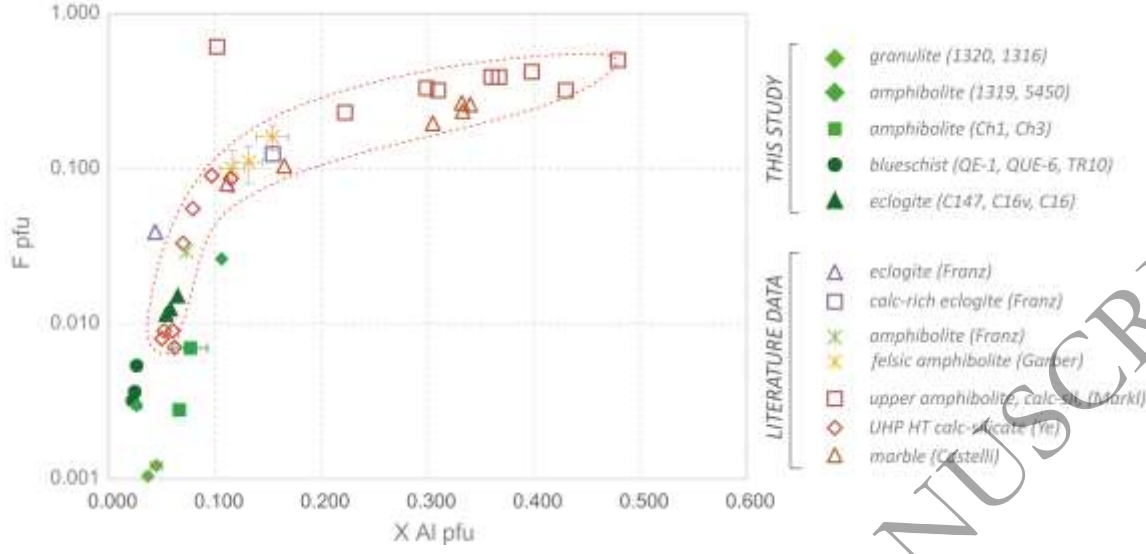

1435

1436

1437

1438 **Fig. 9.**

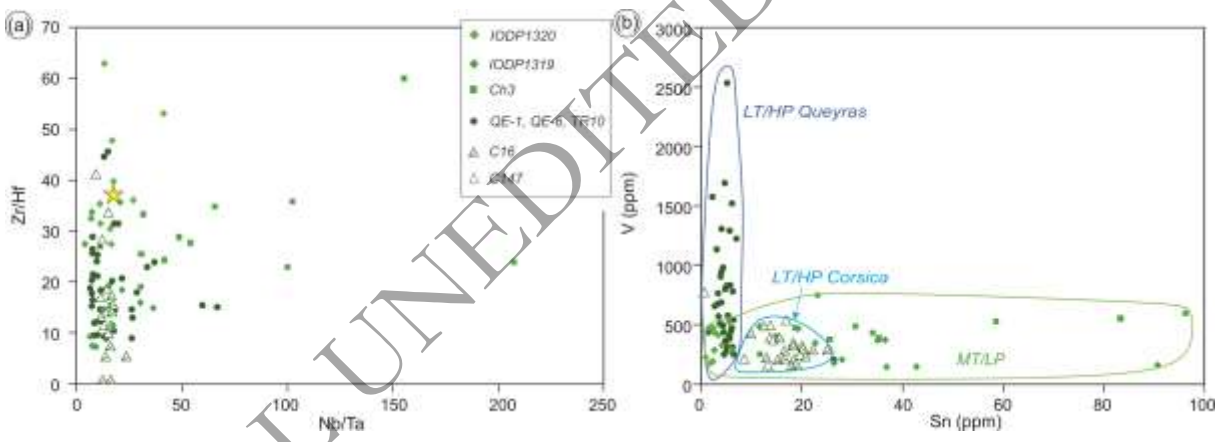

1439

1440

1441

1442

1443

1444

1445

1446

1447

1448

Fig. 10.

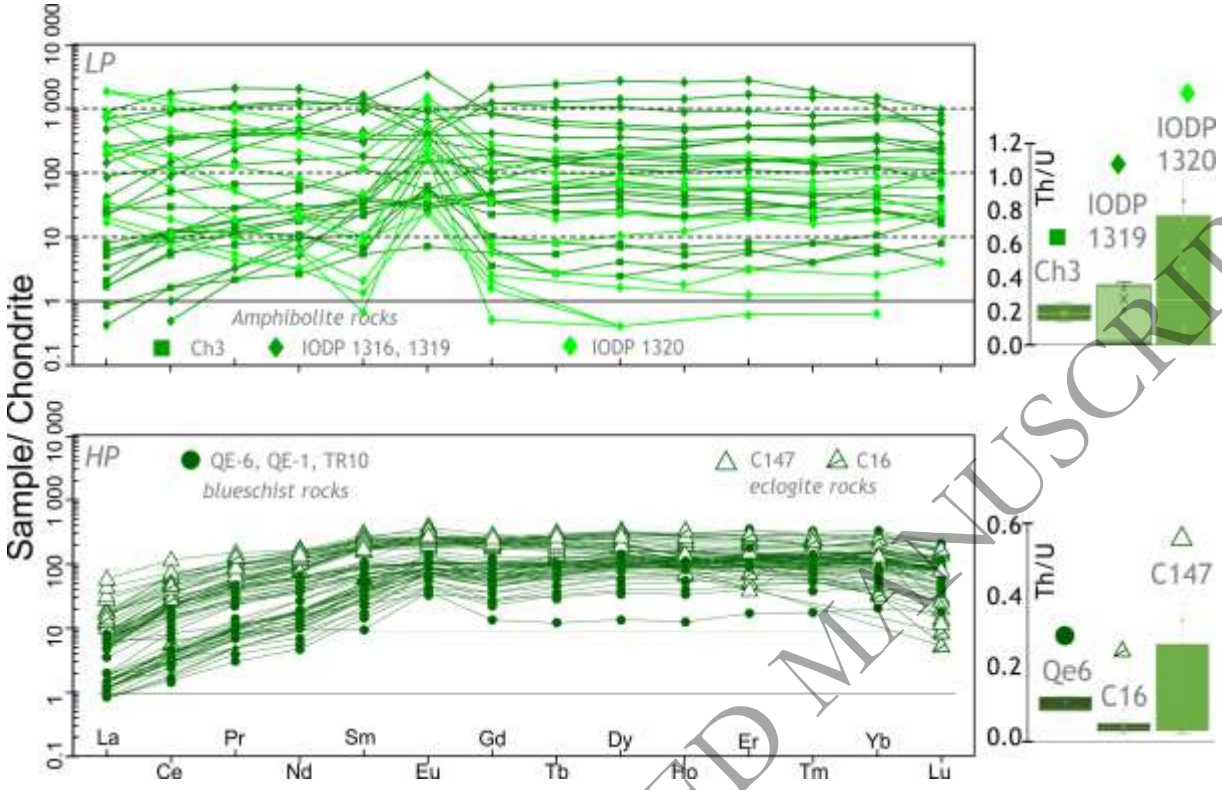

Fig. 11.

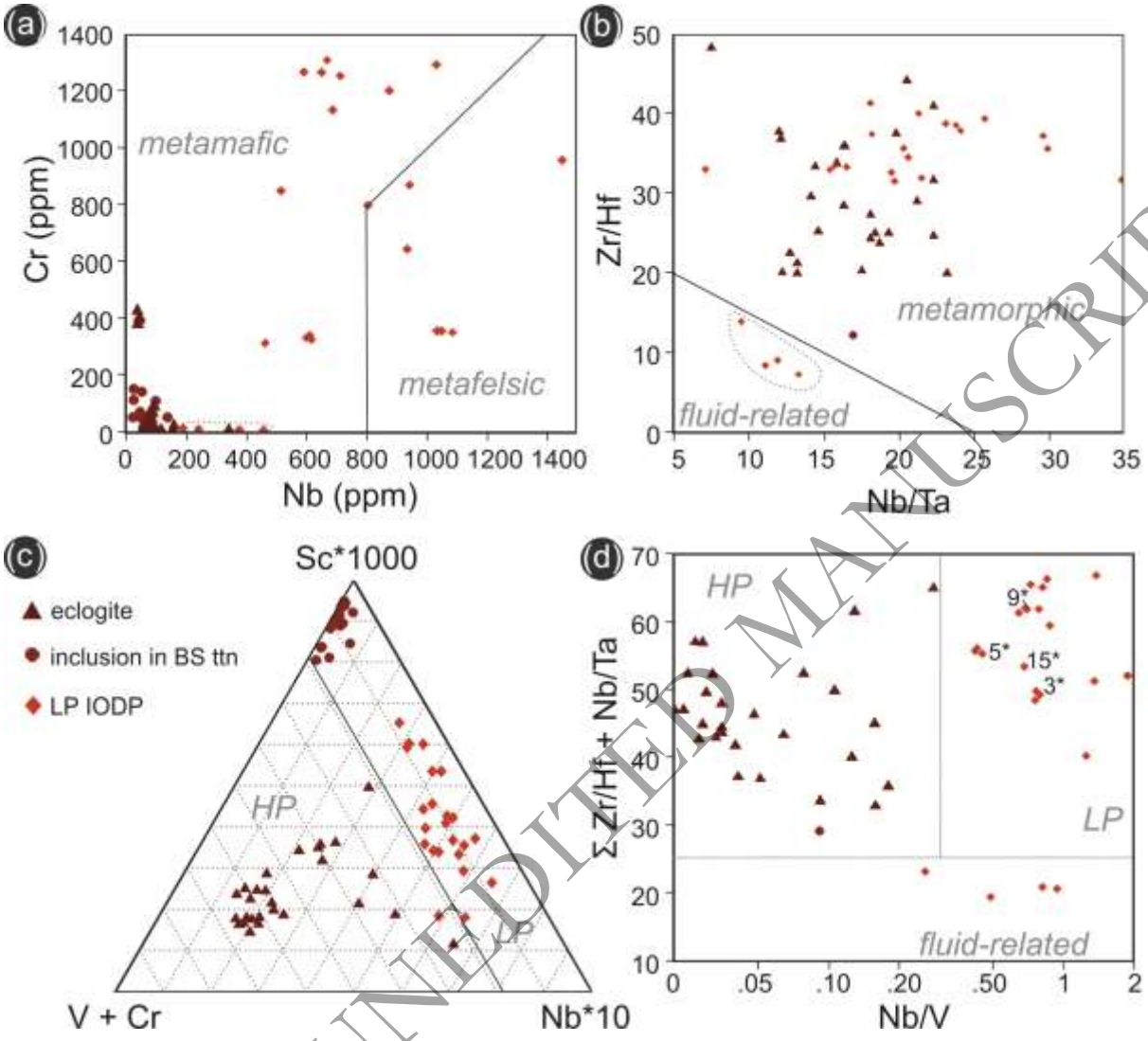

Fig. 12.

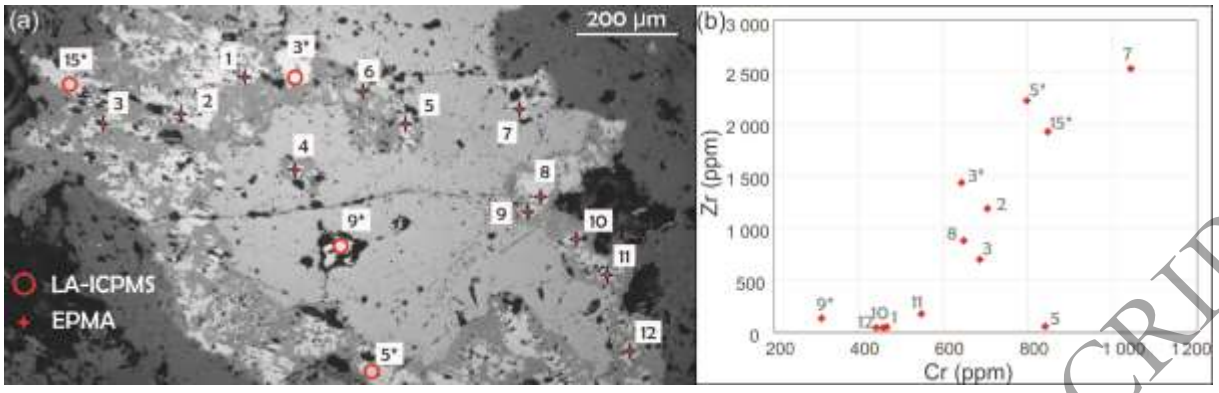

1504 **Fig. 13.**

1505

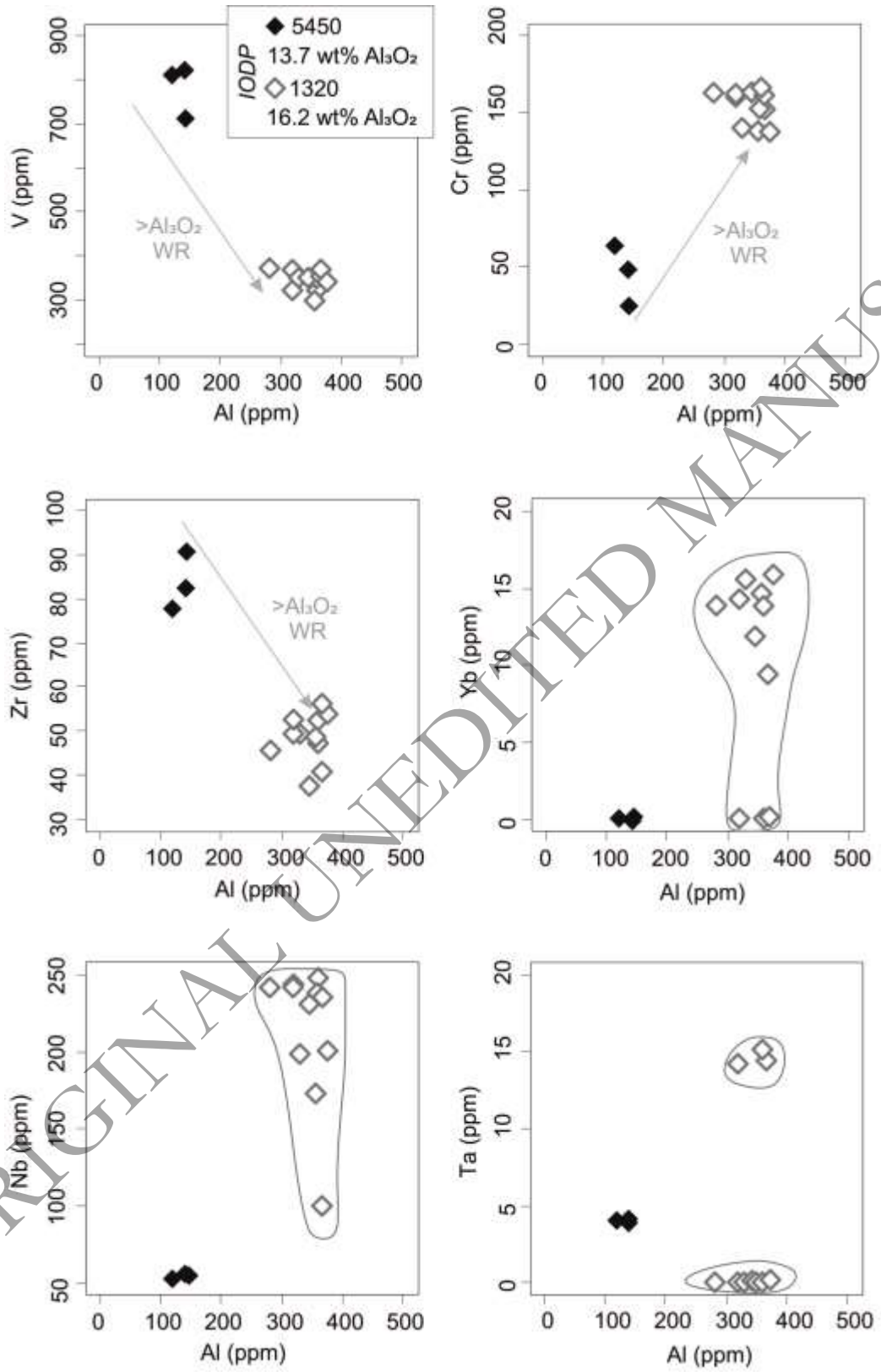

1506

1507

1508 **Fig. 14.**

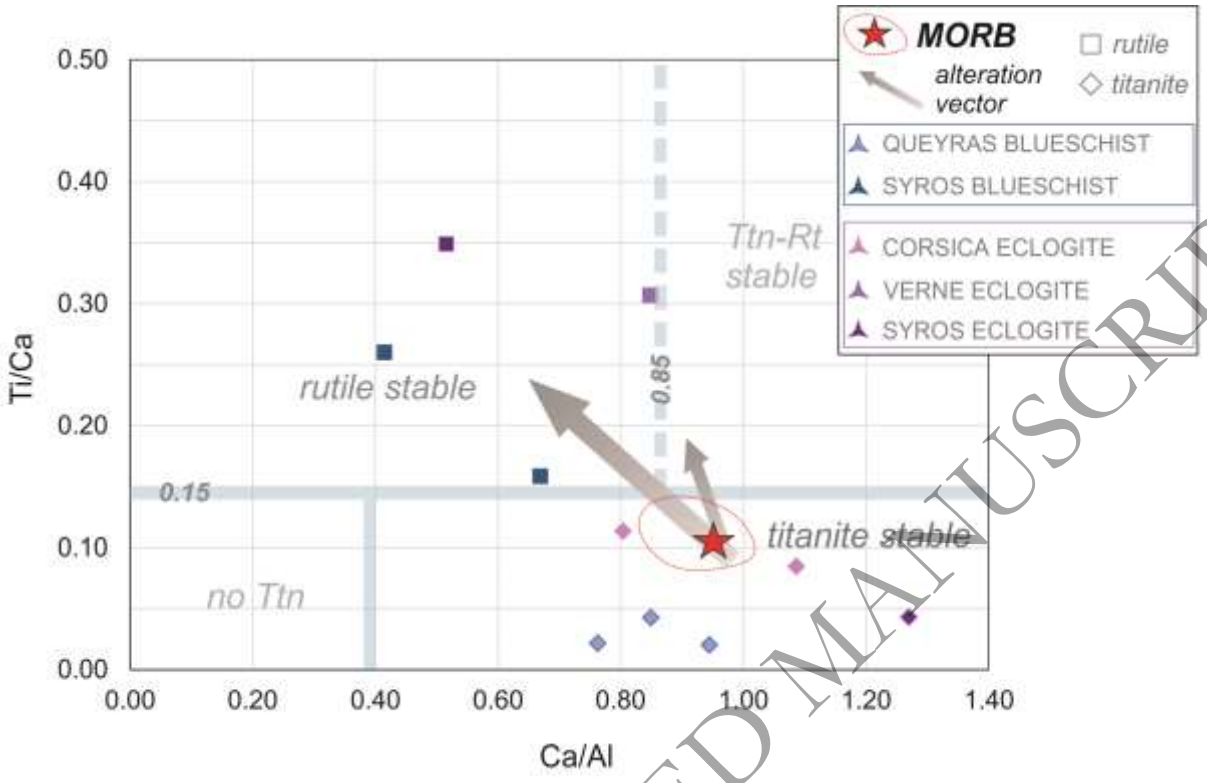

1509

1510

1511 **Fig. 15.**

1512

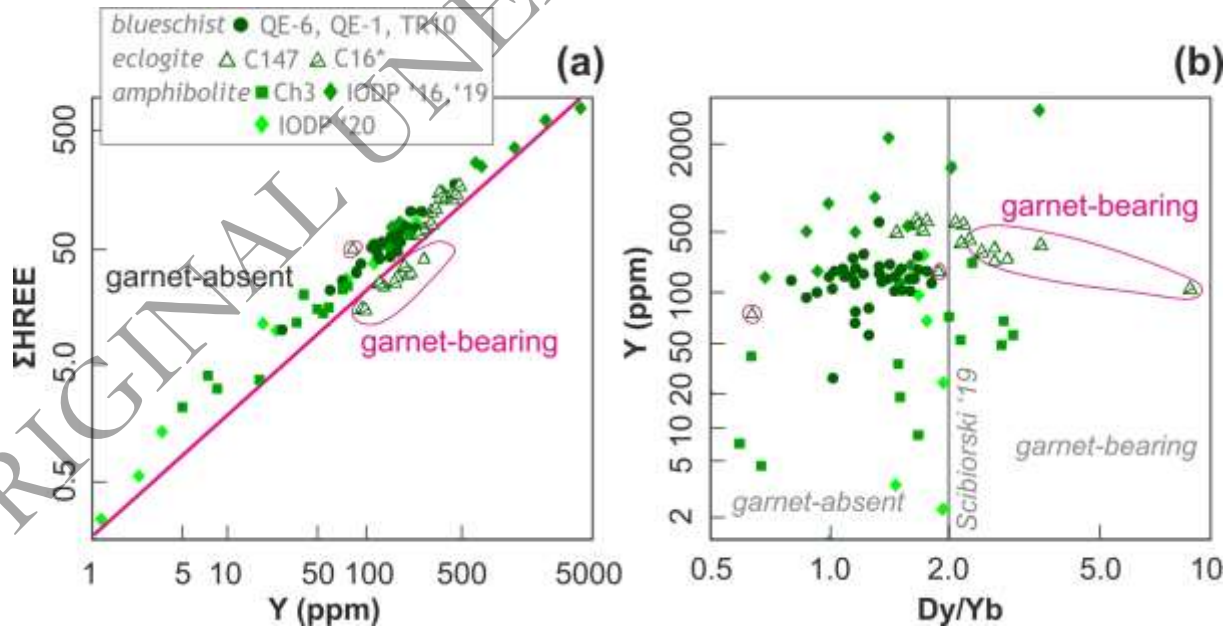

1513

1514

1515

1516

Fig. 16.

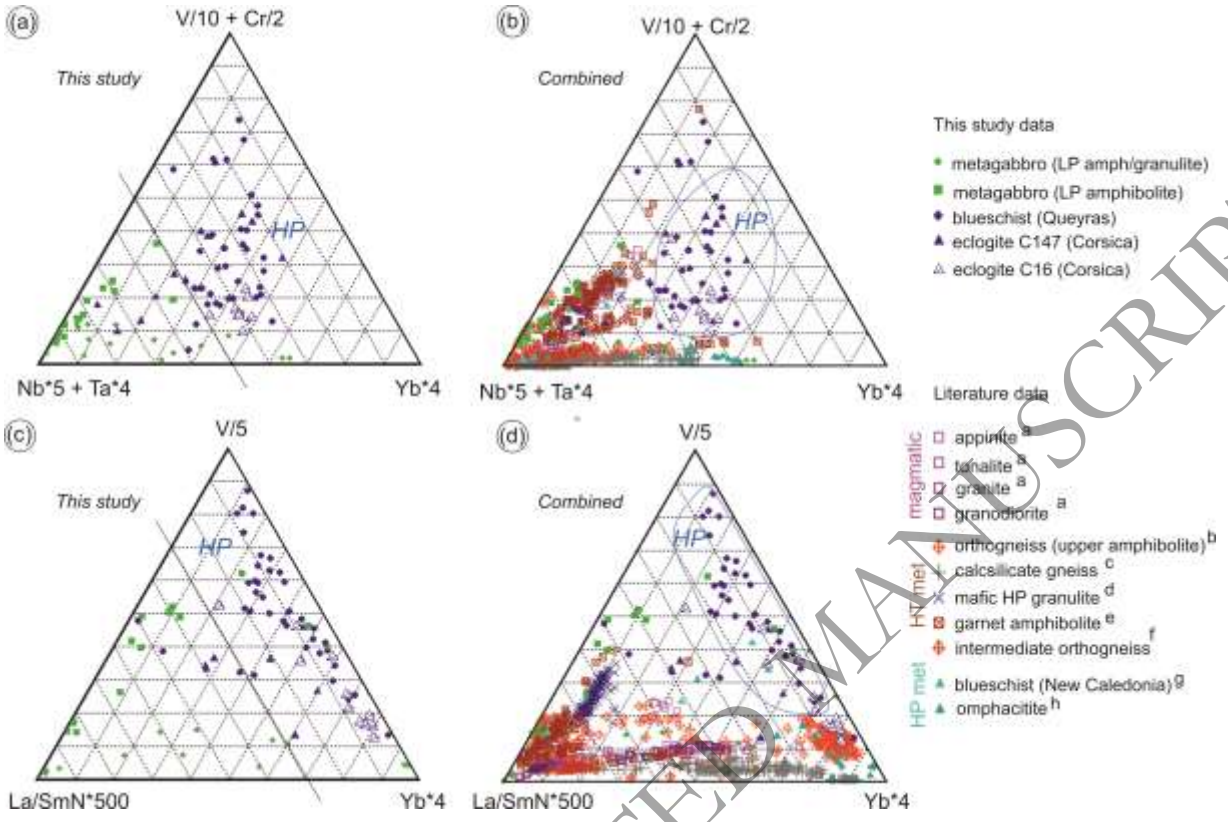

Fig. 17.

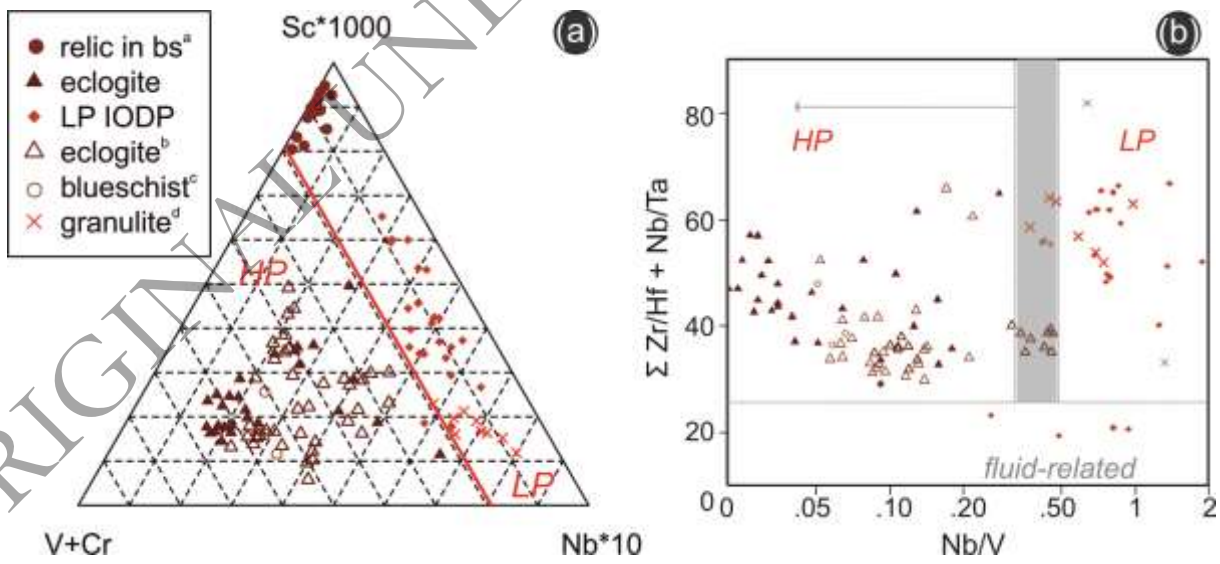

1526 **Fig. 18.**

1527

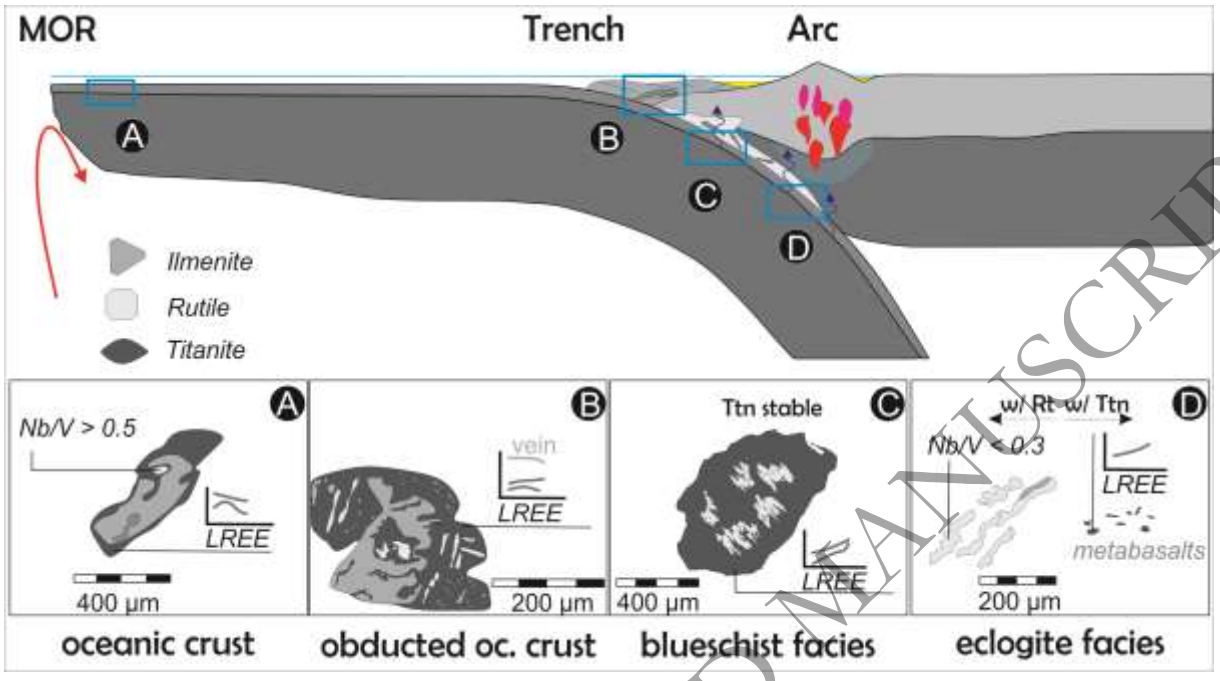

1528

1529